INSTITUTE OF TECHNOLOGY

AIR UNIVERSITY

UNITED STATES AIR FORCE

SCHOOL OF ENGINEERING

WRIGHT-PATTERSON AIR FORCE BASE, OHIO

AF-WP-B-SEP 60 5M

A STUDY OF SHOCK WAVES MOVING OVER A PERFORATED WALL

THESIS

Presented to the Faculty of the School of Engineering of

the Institute of Technology

Air University

in Partial Fulfillment of the

Requirements for the Degree of

Master of Science

By

Robert M. Cameron, B. S.

Capt USAF

Graduate Astronautics

August 1960

Preface

The original requirement for this study of shock interaction with perforated walls was stimulated by several unanswered questions brought to light by shock tube studies of combustion problems and of pressure transducers, which were recessed by gauge lines. No attempt has been made to duplicate the conditions of any one preceding experiment. However, a general investigation of the problem as a whole has been carried out, during the time available for the study, to try and shed some light on a rather complex phenomenon.

As man attempts to travel faster and higher, he continually runs into perplexing new problems in gas dynamics. Shock wave generation and propagation in complicated ducting which might utilize perforations, such as flame cans, boundary layer energizers, and thrust augmentation devices, are just some of the many facets of these problems whose solutions might be aided by this study.

This thesis topic was suggested by Doctor Andrew Shine, my faculty advisor, whose guidance, understanding, and aid was a stimulating inspiration during this study and the subsequent preparation of this report.

I would also like to acknowledge the cheerful, willing, and patient assistance given to me by my laboratory assistant, Mr. John Parks, whose technical knowledge and ingenuity helped in the solution of many problems.

I am deeply indebted to Mr. Geoffrey A. Gass, Field Engineer for Tektronix Inc., whose willingly given technical advice and personal assistance were invaluable during the electronic instrumentation phase of this study.

Contents

List of Figures

Figure Page

List of Tables

List of Symbols

A	Cross sectional area of shock tube
C	Velocity of sound, ft/sec.
k	specific heat ratio
$\dot{m}$	Mass rate of flow
M	Mach number of the shock wave
p	pressure , psi
P	Pressure ratio
t	Time after disturbance
T	Temperature, degrees Rankine
u	Velocity, ft/sec
W_s	Velocity of the shock wave relative to the shock tube, ft/sec.
x	Distance along the shock tube from the disturbance.
Z	Percent Attenuation, %.
α	Shock trailing angle, degrees
Δ	Change
ρ	Density

Subscripts

1. Low pressure region in front of shock wave
2. High pressure region behind shock wave in front of contact surface.
3. Region between contact surface and expansion wave.

4. High pressure region before diaphragm rupture.

21 indicates a ratio, i.e. $P_{21} = \frac{P_2}{P_1}$

i initial

s Pertaining to the shock wave.

Abstract

This study investigated the possible effects upon a shock wave moving over a pair of perforated test plates which were open to the atmosphere in the top and bottom walls of a shock tube. The effects of interest to this study were the shock strength, defined as the pressure ratio across the shock, and the shock orientation, indicated by the normality or obliqueness of the wave to the direction of flow. The number and size of the holes for a given open area, the open area, the rate of flow in through the perforations prior to shock passage, and the strength of the incident shock wave were all varied to determine the effects of these parameters. The results of this investigation showed that the strength of the shock wave, after being disturbed, was affected by the time required to establish the flow of air out through the perforations by the high pressure air behind the shock. If the holes were small, or flow out was established with some difficulty, the reflected shock waves formed at the openings of the perforations were observed to retard the attenuation of, or even strengthen, the incident shock wave. This occurred during a time lag before expansion waves, generated by the loss of mass out through the preforations could weaken the shock. These observations, made with pressure measuring instruments, were verified by the Schlieren photography.

A STUDY OF SHOCK WAVES MOVING OVER A PERFORATED WALL

I. Introduction

Background Information

The first recorded use of a shock tube was in 1899 by the French scientist, Paul Vierlle, and in the years that followed, much of the basic shock tube theory was developed. However, experiments were limited by the instrumentation available to record the short time duration runs, and it was not until the advent of accurate electronic instruments and high speed photography equipment that the shock tube could become a useful aerodynamic testing facility.

In the past decade, the shock tube has been used to investigate many problems in physics and fluid mechanics. Aside from its use as a short duration wind tunnel, it has proved valuable for studying the shock loading of structures, the physical effects produced in gases at extremely high temperatures, and combustion and flame propagation.

Problems that have developed in studies of the latter type have established the requirement for this present investigation. Experiments (Ref 6) have been conducted to determine the effect of a moving shock wave on flame fronts in combustion chambers that required an exhaust system to be used in conjunction with a shock

tube. The exhaust system utilized perforations in the walls of the shock tube, and the results of the experiments were considered inconclusive, because the properties of the shock wave after passing over the perforations were not known and had to be assumed.

Purpose

The purpose of this study is to determine experimentally what effect perforations in the walls of a shock tube have upon the characteristics of an incident shock wave.

The characteristics that are of interest in this study are the shock wave orientation and the shock strength. The shock orientation is the geometric relation, either normal or oblique, between the shock wave and the direction of flow. Theoretical analysis (Ref 8:238), assuming one-dimensional unsteady flow, defines shock strength as the ratio of pressure, temperature, or density of the gas immediately behind the moving shock wave to that ahead of it. The Mach number of the wave is also considered a measure of its strength.

The perforations studied were holes placed normal to the flow in test plates which were set in flush with the upper and lower walls of the shock tube. These holes were machined into the test plates in such a manner that their entrances on the inside surface of the walls were sharp and unbeveled. The holes were open to the atmosphere on the outside surface of the plates.

Scope of the Study

Several conditions were studied to determine their effect on the shock wave. The total open area of the perforated plates, for a given hole size, and the size of the holes, for a given area, were varied. Also the rate of flow was varied for air drawn into the shock tube through the perforations. In addition, the effects of a slot were investigated and compared to perforations of the same open area. The strength of the incident shock wave was also varied to determine what noticeable effect this has upon the attenuation.

In the following chapters the phenomenon is discussed, and possible effects, based on previous theoretical and experimental analysis, are presented. A plan of investigation based on this discussion is outlined, and the apparatus used and the experimental procedures employed for this study are described. The results of the experiment are then analyzed, discussed, and summarized, and recommendations made. Also included for clarity in this report are an appendix, with appropriate sample calculations, tables, graphs, drawings, and photographs.

II. Preliminary Discussion

Basic Shock Tube Theory

The basic shock tube relations, developed from one-dimensional unsteady flow theory, are universally accepted as describing the generation and the properties of a moving shock wave. The phenomenon will be summarized here to clarify some of the terms and relationships relevant to this study. (Ref 7:5-108)

The basic shock tube, shown in Fig. 1, consists of a long constant cross sectional area tube and a diaphragm, which initially separates a low-pressure region, 1, and a high-pressure region, 4, of the tube. These pressures are p_1 and p_4, respectively. The temperatures of regions 1 and 4, T_1 and T_4, are assumed equal. When the diaphragm is ruptured, a shock wave and a rarefaction wave are generated which accelerate the gas in regions 2 and 3. The shock wave propagates into region 1 and the rarefaction wave travels into region 4. The velocity and pressure of the gas in region 2, u_2 and p_2, equal the velocity and pressure in region 3, u_3 and p_3. Due to the properties of the rarefaction wave, there is no entropy change between regions 4 and 3. Therefore, the temperatures of regions 2 and 3, T_2 and T_3, are not equal, and a contact discontinuity must exist to separate the high temperature gas of region 2 from the low temperature gas in region 3.

The shock wave velocity relative to the shock tube and also to region 1, whose velocity, u_1, is zero, is W_s, and the Mach

number, M_s, of the shock is therefore equal to W_s divided by the speed of sound in region 1, C_1.

The equations of state, energy, momentum, and continuity have been used to derive the differential equations describing this phenomenon. These equations have been solved, and the resulting relations have been used to determine all the properties in each of the four regions. Glass (Ref 7:5-108) and Shapiro (Ref 12: 922-1027) are just two of many good references that present the solutions of the equations. It is therefore possible, given the ratio p_4 to p_1, P_{41}, to determine the theoretical ratio, P_{21}, and once P_{21} is known all the other properties of the regions can be determined.

One-Dimensional Flow Assumption

The basic assumption for most of these derived relations is, of course, one-dimensional flow, but the effects of a perforated wall on a shock wave are more than one-dimensional, since the entire cross-section of the shock is not being affected at the same time. However, one-dimensional analysis may be used to determine the characteristics of the shock wave. This assumption is substantiated by the many theoretical and experimental studies that have been made to correlate experimentally obtained shock tube flow measurements with viscous unsteady flow theory (Ref 9:2). The assumption is made that the flow is quasi-one-dimensional, and the wall boundary conditions are included in the flow conditions, which are averaged

across the tube at representative cross sections of the flow. These averaged cross-section properties are then included in the one-dimensional theory.

The Shock Wave Strength

The properties in region 1 are assumed constant throughout the process. Therefore, the properties in region 2 are of primary interest to this study, because the ratio P_{21} defines the characteristics of the shock wave and may be considered the strength of the shock.

The expression for the shock wave pressure ratio as a function of the shock Mach number, M_s, and the specific heat ratio, k, is

$$P_{21} = 1 + \frac{2k}{k+1} \left(M_s^2 - 1 \right) \qquad (1)$$

When the gas considered is air, whose k equals 1.4 approximately, this relation reduces to

$$P_{21} = \frac{7M_s^2 - 1}{6} \qquad (2)$$

Attenuation Measurements

Huber and McFarland (Ref 9:20-22) describe a method for calculating the attenuation of a shock wave which has been adapted to this investigation.

The difference between the shock strength before and after being disturbed is considered the shock loss due to the disturbance and is $\frac{\Delta p_2}{p_1}$.

The shock-pressure attenuation, z, is

$$z = \frac{\frac{\Delta p_2}{p_1}}{\frac{p_2}{p_1} - 1} \tag{3}$$

When this is multiplied by 100 percent, the percent attenuation, Z, is obtained.

$$Z = \frac{\frac{\Delta p_2}{p_1}}{\frac{p_2}{p_1} - 1} \times 100\% \tag{4}$$

When Z is positive a decrease in the shock strength has occurred, and when Z is negative the shock wave has been strengthened.

Attenuation of a Shock Wave in a Tube

A discussion (Ref 5:4-8) of the relation between the mass flows associated with the shock movement is summarized here and modified for this investigation.

When the diaphragm is burst the entire mass of air in the region between the expansion wave and the shock wave is set into motion at a velocity equal to u_2. This initial mass rate of flow, $\dot{m}_1$, for a given shock tube cross-section area, A, is

$$\dot{m}_1 = \rho_2 u_2 A \tag{5}$$

However, the flow in the region behind the shock wave may decrease, because of boundary layer action or some other disturbance. Therefore, this flow at anytime maybe expressed as

$$\dot{m} = \rho_2 u_2 A f(t,x) \qquad (6)$$

Where $f(t,x)$ may be a function of time and the distance which has elapsed after passing over a disturbance.

In addition, the shock wave itself sets into motion a mass flow, $\dot{m}_s$, which is related to the pressure ratio across the shock wave by the following expression:

$$\dot{m}_s = \rho_1 C_1 A \frac{5}{7} \sqrt{6P_{21} + 1} \; \frac{P_{21} - 1}{P_{21} + 6} \qquad (7)$$

Whenever $\dot{m}_s$ is greater than $\dot{m}$, an expansion wave is generated which travels at the local speed of sound and catches up with the shock wave, reduces its strength, and thus equalizes the flow. Conversely, if $\dot{m}_s$ is less than $\dot{m}$, a compression wave is generated, and the strength of the shock is increased to equalize the flow.

Attenuating Effects of a Perforated Wall

Let us visualize the flow in a tube after the shock has passed over the perforations. Since the pressure in the region behind the shock wave is obviously higher than atmospheric, there will be a flow out through the holes. NACA (Ref 2:5), after conducting a series of experiments with air flow through perforations, concluded that the primary factor affecting the quantity of air flow for a given pressure differential was the open area. The number of holes, the hole depth, and the shape of the individual holes had little or no effect on the flow.

The loss of mass flow behind the shock wave will cause $\dot{m}$ to become less than $\dot{m}_s$ and expansion waves will be formed which,

in turn, will weaken the shock. From this discussion, it would appear that the attenuation of the shock wave is proportional to the mass flow out through the perforations.

Transition Period to Establish Quasi-Steady State

However, the preceding conclusion is based on the assumption of a quasi-steady flow and assumes that the boundary conditions for a non-steady flow are the same as for a steady flow. In reality though, when steady flow boundary conditions have been disturbed by a pressure wave, they are only re-established by a system of reflected waves during a finite time lag. This was shown by Rudinger (Ref 11:1-6) who experimentally studied the effects of orifices at the end of a shock tube. He found that the effects of this time lag, often neglected in conventional analysis, are greatest when the disturbing wave is a shock wave; and that the properties of the flow during this transition period, during which compression and shock waves were generated, are completely different from those during the quasi-steady state period. Therefore, there is the possibility that, before the quasi-steady flow out through the perforations can be established, some other phenomena may occur which will generate waves other than the expansion waves caused by the loss of flow.

Crichton (Ref 1:23-24), studied the pressure response of a transducer placed at the end of a tube or gauge line, which was oriented at right angles to the shock tube. He was essentially

working with a single, closed-end perforation. He assumed and showed by his experiments that, when the primary shock wave was incident upon the mouth of the gauge line, a shock wave was generated which traveled up into the line.

The generation of this shock wave was compared to the bursting of a diaphragm at the mouth of the gauge line and thus related to the one-dimensional shock tube theory. Although he made no attempt to analyze the effect produced by the gauge line on the primary shock wave, his study did discover that the induced shock wave in the gauge line was, in all cases examined, weaker than the primary incident wave, and that the shape of the entrance to the gauge line also affected this strength. It was noted that a stronger shock wave, though still weaker than the incident wave, was induced in the line if the entrance to the mouth of the gauge line was smooth and bell shaped than if it was sharp and normal to the shock tube. This would indicate that flow was established easier through the bell-shaped entrance. Therefore, it is believed that the ease with which the flow is established through the perforations has a transient effect on the strength of the incident shock wave due to the time lag generated and its associated phenomena. If reflected shock waves are generated during this transition period, there is the possibility that the primary shock may be initially strengthened by them before any attenuating expansion waves can be generated by the out-flow.

Shock Wave Orientation

It is of interest to know what effect the perforations will have on the orientation of the shock waves. Although the perforations present no obstructions up into the tube, it might be possible to relate them to two sharp-cornered discontinuities: initially as the shock boundary enters the hole and then as it leaves. This may be assumed since the thickness of the shock wave is many orders of magnitude less than the dimensions of the holes. Sun (Ref 14:12) predicted mathematically what happens when a shock wave is incident upon a right-angled edge such as those presented by the sharp-cornered perforations. The strength of the disturbed part of the incident wave was increased by the reflected shock waves, but in order to satisfy both the normal and tangential boundary conditions, the face of the shock wave did not remain normal to the flow. This condition is believed to be just a temporary one, and the shock front will again normalize itself by equalizing the strength across its face.

NACA (Ref 9:20) investigated the shape of a shock wave during its formation after diaphragm rupture and noted that the shock wave was not one-dimensional and normal to the flow at first. However, as it progressed downstream it became normal to the flow and this orientation appeared to be its equilibrium shape.

The Effect of a Flow of Air in Through the Perforations

The flow of air, drawn through the perforations by the exhauster at the end of the tube, is cut off as soon as the shock wave crosses the holes. However, there is believed to be a certain amount of inertia associated with the mass of the air flowing in toward the shock tube at cut-off. This inertia must be overcome before the flow can be reversed and established outward. This effect should also contribute to a time lag.

On the other hand, the flow of air will have a boundary layer associated with it in the holes as well as in the shock tube downstream of the perforations. In the shock tube, this boundary layer, starting at the perforations and proceeding downstream, can be viewed as a disturbance or viscous effect which slows the flow, $\dot{m}$, associated with the incident shock wave, and thus generates expansion waves. However, this boundary layer could also be considered a reduction in the effective cross-section of the tube. The results of an experiment published by the Rand Corporation (Ref 10:829) show that the pressure ratio, P_{21}, of a shock wave transmitted through a reduction in area can be increased almost linerarly with an increasing pressure ratio of the incident shock for a given contraction.

Summary of Possible Effects

It can be summarized from this preliminary discussion that the effects of the perforations and the flow of air in through them

is complicated by the many possible phenomena that can occur. All of these could be present at different times to either strengthen or weaken the incident shock wave and change its orientation. Initially, a reflected wave could strengthen the primary shock and change its orientation, but as soon as the flow is established out through the perforations, the resulting loss of mass behind the shock wave would generate the required expansion waves to equalize the mass flow. These expansion waves would then decrease the strength of the primary incident shock wave. The flow of air initially in through the holes could either contribute to the length of the transition period, thereby decreasing the rate of attenuation, or increase the attenuation with its viscous properties.

III. Description of Apparatus

Experiments were conducted to explore the afore-mentioned possible effects of the perforations and air flow upon the incident shock wave. In order to accomplish this, the strength of a shock wave, P_{21}, was determined before passing over the perforations and then it was compared to the strength of the same shock wave downstream of the perforations to determine the attenuation of the shock wave. Schlieren photographs were made of the shock wave as it passed over the perforations to determine if the shock wave's orientation was changed and to study the flow immediately behind the wave. The following parameters were varied: the strength of the incident shock wave, the hole size, the open area, and the flow in through the perforations.

The facilities of the Institute of Technology's Mechanical Engineering Laboratory were used to conduct these experiments. Figure 2 is a schematic drawing of the test equipment and Figure 3 shows a general view of the shock tube. The following is a detailed description of the individual components used to acquire the necessary data.

Shock Tube

The Institute of Technology's shock tube was designed in 1955 and is described in Ref 3. The basic, unmodified tube (Fig 2) whose inside cross section is a rectangle, four inches by eight

inches, is 20 feet long and is composed of five four-foot long sections. Section 1 is the high pressure section, and a Mylar film diaphragm is clamped between sections 1 and 2 by two hydraulic cylinders which are capable of 2000 psi pressure each. Section 5 is the normal test section and has a set of six-inch diameter, optically flat glass viewing ports in its sides. Section 5, which is mounted on a caster-wheeled support, was disengaged from section 4 for this experiment and moved downstream to allow an 18-inch long test section (Fig 4) especially designed for this study, to be placed between sections 4 and 5.

Section 4 contains three receptacles in which pressure transducers may be mounted. These are located 100 in., 128 in., and 140 in. downstream from the diaphragm and are designated stations A, B, and C respectively for this study.

Section 5 was modified by the addition of two more transducer receptacles located 3-7/8 in. and 28 in. from the upstream end of section 5. These are designated stations D and E, respectively.

The driver gas for this study was dry, oil-free air delivered by the laboratory's compressed air system. Since the perforations were open and exhausted to room atmosphere, the low pressure section could not be evacuated, and the driven gas was, therefore, air at room conditions.

Test Section

The special test section, Fig 5, was designed so that its

inside dimensions would match the shock tube's inside cross section and mate flush with sections 4 and 5. However, on the outside, the two vertical side plates were extended four inches above the shock tube to mount two six inch diameter, optically flat glass view-ports, whose centers coincided with the top inside wall of the test section. This configuration was used to achieve the maximum field of vision at the top wall for Schlieren photography.

Two openings, Fig 6, which measured 6 in. x 4 in. in the outside faces and stepped down to 4 in. x 4 in. in the inside faces of the top and bottom walls, were used to hold the various pairs of test plates as shown in Fig 7. Both the test plates and the test section were fabricated from one inch thick aluminum jig plate.

Test Plates

Eleven different configurations of test plates were used. The different perforation geometries were machined into the four inch by four inch face of five different pairs of plates. These plates were milled to within a tolerance of $\pm$ .002 inch of each other and to a forced fit into the openings in the test section. Every precaution was taken to eliminate any disturbances to the flow that might be caused by the plates or the test section.

Figures 8, 9, and 10 are representative pictures of the test plates used. The following is a list of the geometries tested:

1.) Blank plates

2.) Open area each plate .491 $in.^2$

a. .125 in. slot

b. 40-.125 in. diameter holes per plate

3.) Open area each plate .589 $in.^2$

a. 3-.50 in. diameter holes per plate

4.) Open area each plate .982 $in.^2$

a. .25 in. slot

b. 80-.125 in. diameter holes per plate

c. 20-.25 in. diameter holes per plate

d. 10-.35 in. diameter holes per plate

e. 5-.50 in. diameter holes per plate

5.) Open area each plate 1.964 $in.^2$

a. 10-.50 in. diameter holes per plate

6.) Open area each plate 3.928 $in.^2$

a. 20-.50 in. diameter holes per plate

All perforations presented sharp, unbeveled openings to the flow. The two slotted configurations were counter-milled, and all the holes, except those with .50 inch diameters, were counter-drilled so that the effective lengths of these perforations were only 5/16 inch.

A geometric pattern was chosen for each size and number of holes such that the entire width of the shock wave would be affected, and when possible, the holes were distributed equally over the face of each plate.

Exhaust System

Figure 11 is a general view of the exhaust system, which consists of three basic components: the exhauster, the exhaust hose, and the flow meter.

Exhauster. The prime mover for the exhaust system was a cabin heater blower for a C-54 aircraft. This unit consists of a turbine blower driven by a ½ horsepower, 28 volt DC, electric motor rated at 25 amps. Power was supplied to this motor by a 115 volt AC driven, 40 amp. "Variac" through a silicon diode rectifier. This arrangement allowed the flow to be varied by changing the motor speed with the Variac.

Exhaust Hose. A two inch inside diameter, helical wire supported, neoprene and fibre-glass, flexible hose was used between the exhauster and the end of the shock tube. This hose, which is rated to withstand a pressure differential of 16 psi, was purposely bent into a 180 degree arc to dissipate the shock which entered it from the end of the shock tube.

Flow Meter. The end plate of the shock tube was removed and replaced with a flow meter which was designed for this study. This is a nozzle whose entrance geometry is based on the revolution of an empirically derived ellipse (Ref 4:644-647). The discharge coefficient for this type of meter, at the flows encountered during this experiment, is 0.988.

Manometers

The high pressure readings upstream of the diaphragm were obtained with a 150 inch mercury manometer and the low pressure readings in region 1 were obtained with a 30 inch water filled U-tube manometer.

The changes in pressure across the flow meter were indicated on a 4 inch, inclined manometer, which was filled with Meriam oil, but calibrated to show pressure differences in inches of water. When flows with pressure differentials greater than four inches were encountered, a 30 inch, water filled, U-tube manometer was used.

Transducers

All pressure steps of the shock waves were measured directly with Endevco Corporation Model 2501-500 piezoelectric transducers. The output of these transducers is a voltage which is linear with the pressure step that is impressed upon them. These transducers are ruggedly constructed and are designed to operate in a steady state temperature range between (-) 30 and + 80 degrees C. up to their rated values of 30 volts at 500 psi.

Transducers with serial numbers 17, 18, 16, and 15 were mounted flush with the flow at stations B, C, D, and E, respectively for the experimental runs. The transducers were calibrated prior to the experimental phase of this study.

Manometers

The high pressure readings upstream of the diaphragm were obtained with a 150 inch mercury manometer and the low pressure readings in region 1 were obtained with a 30 inch water filled U-tube manometer.

The changes in pressure across the flow meter were indicated on a 4 inch, inclined manometer, which was filled with Meriam oil, but calibrated to show pressure differences in inches of water. When flows with pressure differentials greater than four inches were encountered, a 30 inch, water filled, U-tube manometer was used.

Transducers

All pressure steps of the shock waves were measured directly with Endevco Corporation Model 2501-500 piezoelectric transducers. The output of these transducers is a voltage which is linear with the pressure step that is impressed upon them. These transducers are ruggedly constructed and are designed to operate in a steady state temperature range between (-) 30 and + 80 degrees C. up to their rated values of 30 volts at 500 psi.

Transducers with serial numbers 17, 18, 16, and 15 were mounted flush with the flow at stations B, C, D, and E, respectively for the experimental runs. The transducers were calibrated prior to the experimental phase of this study.

Electronic Instrumentation

Two different oscilloscopes, Fig 12, were utilized for this study: a Tektronix Type 531 and a Hickok Type 1805.

Type 531 Oscilloscope. A Tektronix Type 531 oscilloscope with a Type 53-54D vertical deflection plug-in preamplifier and a Type 123 trigger preamplifier was used during the calibration and experimental runs to obtain a voltage vs. time plot from two transducers. This oscilloscope achieves a one percent horizontal sweep rate accuracy throughout its complete range from .02 microseconds per cm. to 12 sec. per cm. The vertical deflection system, with the Type 53-54D preamplifier allows the differential presentation of two different channels of signals within a two percent deflection accuracy. The Type 123 preamplifier amplifies, 100 times, a trigger signal from a transducer to start the oscilloscope's sweep. This particular oscilloscope had been modified to include a single sweep circuit which prevents any retriggering of the sweep after the shock wave has passed over the triggering transducer.

Type 1805 Oscilloscope. A Hickok Type 1805 oscilloscope, with a Tektronix Type 53-B plug-in preamplifier for vertical deflection, was used in conjunction with the Type 531 during the experimental phase of this study. This oscilloscope is the same as a Tektronix Type 545, but is manufactured under a government contract by the Hickok Electric Instrument Company. This oscilloscope is basically a Type 531 with the addition of a sweep delay circuit. This circuit

allows the selection of a variable calibrated time delay that will retard the initiation of the main sweep for a predetermined time, after a trigger has been received.

Oscilloscope Cameras. The entire single sweep presentation of the phenomenon lasted only 500 microseconds. Therefore, the sweep transit had to be recorded photographically, and two Polaroid Land cameras (Fig 13) mounted on Fairchild Model F-296A adapters were used to record the oscilloscopes' displays. Type 42 (ASA200) and Type 44 (ASA400) film were used with equally satisfactory results. The lens openings for both films was F 1.9.

Schlieren System

Figure 14 is a schematic drawing of the optical system used for the Schlieren photography. The light source was a General Electric FT-230 spark lamp, fired by a power supply which was assembled by the technicians of the Institute of Technology's Mechanical Engineering Laboratory from a design presented in Ref 15. This unit was calibrated prior to its use for this study by the Electronic Technology Laboratory of the Wright Air Development Division. The results of the calibration indicated that the useable spark duration was five microseconds with a one microsecond rise time, and the time delay through the power supply to the spark lamp was four microseconds. The total time delay for the light source was therefore five microseconds.

The power unit was triggered by a 150 volt, sawtooth, pulsed signal from the Type 1805 oscilloscope. The rise time for this pulse was one microsecond.

The parabolic mirrors for the system were six inches in diameter and had a 30 inch focal length.

The photographs were taken with a Polaroid adapter back for a Graphlex camera, which was mounted on a simple bellows, Fig 15. No lens or shutter were employed because the pictures were taken in a darkened laboratory. Polaroid Type 44 film proved quite satisfactory for this arrangement.

IV. Experimental Procedures

Two different electronic instrumentation configurations were employed during this study. The first was used during the transducer calibration phase, and the second was used during the experimental runs.

Transducer Calibration Configuration

Fig. 16 is a schematic drawing of the electronic instrumentation used to calibrate the transducers. When the shock wave passed station A, its pressure step caused this transducer to generate a voltage which was amplified by the Type 123 preamplifier. This amplified signal then triggered the sweep of the Type 531 oscilloscope, which presented a trace that was representative of p_1. Figure 17 is a photograph of the trace and an annotated drawing is shown in Fig. 19 interpreting the oscilloscope's presentation. When the shock wave crossed stations B and C, the voltages representing these stations' transducers response to the pressure step were indicated as vertical displacements of the sweep's trace. The horizontal displacement of the sweep was the time history of the phenomenon, and the start of the sweep as the shock wave passed station A, the pressure pulse from station B, and the pressure pulse from station C were all displayed in their correct time sequence by one sweep.

Experimental Runs Configuration

Fig. 20 is a schematic drawing of the electronic instrumentation used during the experimental runs. When the shock wave crossed station B, its transducer triggered the sweep on the 531 oscilloscope. At this instant, a 25 volt, square wave, gate signal, whose rise time was .01 microsecond, was initiated by the 531 and used to trigger the delayed sweep of the 1805. As the shock passed stations C and D, the response from these transducers was displayed by the 531's sweep. Fig. 18 is an oscilloscope photograph of the sweep during an experimental run. After the predetermined time delay, calculated to catch the shock wave in the test section's view-port, a 150 volt sawtooth voltage was generated by the 1805 to trigger the Schlieren system's light source. In the meantime the p_1-reference voltage was being maintained and displayed by the 1805's sweep. When the shock wave passed station E its transducer's response voltage was then indicated by the 1805's sweep. In this way, for a given run, the values for the shock wave's pressure steps at stations C, D, and E could all be recorded and Schlieren photography taken of the shock wave as it passed over the perforations.

V. Evaluation of Data

Interpretation of Oscilloscope Photographs

The oscilloscope photographs, Fig. 17 and 18, are, when read from left to right, voltage vs. time representations of the output of the transducers as the shock waves passed down the tube. The start of the sweep and the vertical deflections occurred as the shock wave passed over the appropriate transducers. It is therefore possible to measure the time required for the shock to travel between transducer stations. This was accomplished by measuring the horizontal distance of the sweep length between the start of the sweep and a discontinuity, caused by the vertical displacement of the sweep by an induced transducer's voltage output. The average velocity of the shock wave, W_s, could then be obtained by dividing the known distance between the stations by the time required for passage.

Likewise, after the transducers had been properly calibrated, it was possible, by measuring the vertical deflection of the sweep, to determine the pressure steps, $p_2 - p_1$, of the shock wave as it passed a station.

All measurements of the oscilloscope photographs were made with proportional dividers. A five to one proportion was used, and it was estimated that the accuracy of this method was well within the one percent horizontal and two percent vertical deflection errors of the oscilloscopes.

Calibration Results

The transducers were calibrated with the electronic configuration shown in Fig. 16. The average velocity of the shock wave between stations A and C, for a given run, was used in conjunction with the temperature, T_1, to determine the Mach number of the wave. Equation (2) was used then to solve for the pressure ratio, P_{21}, from which the pressure step, p_2-p_1, was then obtained. The corresponding voltage deflections of the transducers, Tables I, II, and III, were then plotted for each run vs. the pressure steps to obtain the transducer calibration curves in Fig. 21, 22, and 23. The maximum scatter of points from the average curve is only approximately three percent in the area of interest for the experimental runs.

A set of sample calculations for determining the calibration curves is included in the Appendix A.

Experimental Results

General. The electronic instrumentation for the experimental runs is shown in Fig. 20. The pressure steps at stations C, D, and E were obtained from the transducer calibration curves with the voltages measured on the oscilloscope photographs for each run. The pressure ratio, P_{21}, at each station could then be obtained and the attenuation between stations C and D, Z_D, or the attenuation, Z_E, between stations C and E, were determined from equation (4). A set of sample calculations for the attenuation is included in Appendix B.

Test Section Attenuation Check. Blank test plates were inserted into the test section and a series of 20 runs were made to determine the attenuation caused by the test section without any perforations. Tables IV and V indicate the results of these runs. The average attenuation measured between stations C and D was only one percent, while between C and E the average attenuation was 6.7 percent. Since the value of the attenuation between C and D is within the accuracy of the instrumentation, it is assumed, for comparison purposes between subsequent perforation configurations, to be zero.

Attenuation For 0.491 $in.^2$ Open Area Per Plate. Twenty-six runs were made with a 0.125 in.-wide slot placed normal to the flow and milled through each plate, and thirty-three runs were made with 40-0.125 in. diameter holes dispersed over each of the test plate's face. Both configurations had open areas of 0.491 $in.^2$ per plate. The strength, P_{21}, of the incident shock wave was varied and the resulting attenuations, Z_D and Z_E, were determined. The results of these runs are shown in Tables VI and VII.

Attenuation For 0.982 $in.^2$ Open Area Per Plate. In all, 121 runs were made with an open area of 0.982 $in.^2$ per plate, and an average P_{21} of approximately 1.9. Z_D calculations were made from the strength measurements obtained, as the hole size, and consequently the number of holes, was varied from 80-.125 in. diameter holes to a .25 in. wide slot. The flow in through the holes was also varied from zero to .0375 lbs/sec through the 80 hole

configuration and the resulting Z_D's obtained. Z_D's were also obtained for a flow of .0217 lbs/sec through 20-.25 in. diameter holes. In addition the Z_E's were computed for the 80 hole configuration with zero flow. The results of these runs are exhibited in Tables VIII, IX, X, and XI.

Attenuation for Various Open Areas. The open area for each plate was varied by varying the number of 0.50 in. diameter holes per plate. For these 24 runs, the flow of air in through the holes was zero, and the number of 0.50 in. diameter holes was varied from three to twenty. The results of these runs are in Tables X and XII.

Schlieren Photography. Schlieren photographs were made of the shock waves while they were passing over the blank plate, the 80 holes, the 20 holes, and .25 in. slot. Fig. 24, 25, 27, 28, 29, and 30 are representative Schlieren pictures of the phenomenon. The shock is moving from right to left in the pictures. The apparent double image to the left of the shock wave in Fig. 24, 25, 27, and 28 was due to a slight misalignment of the parallel light through the test section. This misalignment was amplified by a very dark setting for the knife edge, which was necessary to obtain reproducible density gradients and contrast in the pictures. This same effect is discussed and illustrated in Ref 13:12,18.

VI. Discussion of Results

Effect of P_{21} on Z_D

Figures 31, 32, 33, and 34 are plots of attenuation vs P_{21C} for the two different plate configurations with open areas of 0.491 $in.^2$ per plate. From the data obtained, there was no indication that the attenuation varied as a function of P_{21C} for ratios from 1.333 to 2.398. Even with a flow of 0.0217 lbs/sec through the perforations the attenuation appeared to remain constant. However this is a narrow range of pressure ratios and no estimate can be made for stronger waves.

Effect of Time and Distance on Attenuation

Figures 33 and 34 are comparisons of the average attenuations noted at stations D and E for the 40-0.125 in. diameter holes and the 0.125 in. slot. The difference in attenuations between Z_D and Z_E is considerably greater than the 6.7 percent obtained from the blank plates during the attenuation check of the test section. This appears to verify the theory that the attenuation is a function of the time and distance from the disturbance, since any expansion waves generated behind the shock wave will require a finite time, and therefore distance, to overtake the shock wave.

Effect of Hole Geometry

0.491 $in.^2$ Open Area Per Plate. Figures 31 and 32 indicate that there was a sizeable difference between the Z_D's for different hole

configurations for a given open area. Where-as the 40-.125 in. diameter holes caused very little attenuation when there was no flow in through these perforations, the 0.125 in. slot attenuated the shock wave's strength 11.7 percent. This indicated that the hole geometry, for a given open area, had a decided effect on the strength of the disturbed shock wave.

0.982 $in.^2$ Open Area Per Plate. The effect of the hole sizes was investigated more thoroughly when the open area of each plate was doubled and a wider range of hole diameters studied. Fig. 35 represents the average Z_D's as a function of the number of holes for a constant open area of 0.982 $in.^2$ per plate. It was interesting to note that for the configuration with 80 and 20 holes per plate the shock wave was actually strengthened at station D. This indicated that the reflected shock waves, generated by either the hole geometry or the establishment of the outward flow, were sufficiently strong enough to reinforce and strengthen the incident wave. This also demonstrated that a longer time lag was required to establish the quasi-steady flow out through the smaller holes and that the formation of the expansion waves therefore was retarded.

However, Table IX shows that the attenuation of the incident shock wave by the 80 holes per plate was increased from the average Z_D of (-) 8.5, noted previously, to an average attenuation of +12.8 at station E, which is 28 in. downstream of station D. At station E sufficient time had elapsed to allow the establishment of the

outward quasi-steady flow and the resulting generation of the weakening expansion waves, which dissipated the short-lived, increased strength of the incident shock wave.

Figure 36 represents an attempt to correlate the average attenuation of the shock wave with the total perimeters of the holes to see if the total length of all the hole edges had any noticeable effect. As in Figure 35, the relation appears to be approximately linear up to the small diameter holes and then, with the advent of the strengthening of the shock wave, the curve loses its apparent linearity and appears to approach some value asymptotically.

Figure 37 represents the average attenuations at station D plotted vs. their respective hole diameters for the same given open area per plate. After due consideration is given to the scatter of the plotted points, it appears that this relation is a linear one.

Effect of Flow in Through the Perforations

0.491 $in.^2$ Open Area Per Plate. Figures 31 and 32 also show the effect of the 0.0217 lbs/sec flow of air in through the perforations. There was a considerable difference noted between the slot and the 40 holes. Where-as the slot weakened the shock wave at station D more with flow than without it, the 40 holes increased the strength of the shock wave with the addition of flow.

This was a paradox whose only apparent explanation was again related to the ease with which flow was established out through

the perforations. It was interesting to note that for the slot the Z_E averaged 25.2 percent for no flow and 27.5 percent with flow, while for the 40 holes Z_E averaged 12.5 percent for no flow and 13.1 percent with flow. This indicated the Z_E was practically independent of the flow in through the holes prior to the shock wave passage and that this flow in had just a transient effect on the shock strength that was overcome by the expansion waves generated by the quasi-steady flow out through the perforations.

0.982 $in.^2$ Open Area Per Plate. The 80- .125 in. diameter holes per plate configuration was selected to determine the effect of different rates of flow on the shock wave strength for a given perforation geometry. The average Z_D's were plotted vs. their corresponding flow rates in Figure 38. It was noticed that the flow had no apparent effect on the shock strength until after a flow of 0.0125 lbs/sec was reached, and then the shock waves were abruptly strengthened in the same manner as noted earlier for the 40-.125 in. diameter hole plate with flow. A minimum average Z_D of (-) 15.6 percent was then reached at 0.0158 lbs/sec, and then as the flow was increased the attenuation of the shock wave was also increased.

This change from a strengthening to a weakening trend may possibly have been due to a change in the flow in through the perforations from a laminar to a turbulent condition, whose increased viscous properties generated expansion waves which increased the attenuation of the shock wave.

The results of Table XI also show that the average Z_D is decreased from a value of (-) 2.7 percent for no flow, for 20-.25 in. diameter hole per plate, to (-) 5 percent for a flow of .0217 lbs/sec in through the holes. This again indicates that the incident shock wave can be strengthened if the flow in through the perforations is kept low enough to avoid strong viscous effects.

Effect of Varying the Open Area

The open area of the plates was varied by increasing the number of 0.50 in. diameter holes from three to twenty per plate. It was noted in the earlier discussions that, for a given pressure differential on either side of the plates, the quasi-steady rate of loss of mass flow out through the holes behind the shock wave is dependent almost entirely on the open area, and that the attenuation should be directly proportional to this loss of mass. However, Fig. 39 represents the average Z_D's as a function of their respective number of holes per plate. The number of holes of equal diameter per plate is of course proportional to the open area, but the shape of this curve indicates that the relation between Z_D and the open area is not linear as would be expected. It is interesting to note that when Z_D is plotted vs. the logarithm of the number of holes, as in Fig. 40, that the relation appears to be a linear one.

Schlieren Investigation

The Undisturbed Shock Wave. Figure 24 shows a typical Schlieren picture taken while the blank plates were installed in the test

section. In this and all the other Schlieren pictures the shock wave is moving from right to left. In Fig. 24 the shock wave appears to be free from interference and is normal to the blank test plate, which appears as the black horizontal strip just above the middle of the circular viewport.

80- .125 in. Diameter Holes Per Plate Without Flow. Fig. 25 is a representative picture of the shock wave transit over a 80-.125 in. diameter hole plate. It was noted that as the shock passed over the perforations, a series of cylindrical reflected shock waves were formed, which in turn coalesced with the incident shock wave. Fig. 26 is an exaggerated drawing of the phenomenon. The face of the incident shock wave is denoted as LMN, and the envelope of cylindrical reflected waves is denoted as MQ. That portion of the shock wave into which the reflected waves have coalesced is labeled LM. The shock waves emitted through the perforations at the top of the plate into the atmosphere are labeled R.

Close investigation of the Schlieren photographs indicated that the leading edge of the shock wave did not remain normal and plane to the flow, but bent back from the normal at point M towards point N by a trailing angle, α , This was concrete evidence that the incident wave was being accelerated by the cylindrical reflected shock waves. That portion of the incident shock wave where the reflected waves had coalesced was moving faster than the unaffected portion. It is interesting to note that the accelerated portion

remains normal to the plate, while the unaffected portion lags behind, causing the angle, α . This result is in complete agreement with the preliminary discussion and with the attenuation data which indicated an immediate increase in strength for the incident shock wave as it passed over this particular perforation configuration. The average angle, α , measured from greatly enlarged photographs, taken at mid-transit across the plate, for the 80-.125 in. diameter holes without flow was 3. degrees.

80-.125 in. Diameter Holes With Flow. Fig. 27 is a Schlieren photograph of the incident wave passing over 80-.125 in. diameter holes in through which air is flowing at a rate of .0217 lbs/sec. It is interesting to note that the image in front of the shock wave, due to the strong light refraction resulting from the slight misalignment of optics, appears very turbulent when there is flow in through the holes.

The average angle, α , for the mid plate position for this case is 5. degrees. This increase in angle over the preceding case again substantiates the attenuation measurements, which indicated a greater strengthening of the shock wave when the flow rate was increased from zero to .0217 lbs/sec.

20-.25 in. Diameter Holes Per Plate Without Flow. Fig. 28 is a composite picture made from the photographs of three different shock waves of equal initial strength taken at different positions along the plate. This shows the generation of the cylindrical

reflected shock waves, which are coalesceing with the incident shock wave and accelerating it as it passes over the plate, and the development of the flow out through the holes.

The average angle, α , at mid plate for this configuration was only 1.5 degrees. This is in accord with the only slight increase in strength for the shock wave noted from the attenuation measurements, Z_D.

The 0.25 Inch Slot Without Flow. Figure 29 is another composite picture which clearly indicates the forming of the cylindrical reflected shock waves as the incident shock waves pass over the 0.25 inch wide slot. The presence of many holes complicated the pattern of these waves in the previous pictures, but with just one slot present, the transition of the wave pattern is now very apparent. The first picture is the undisturbed incident wave just prior to striking the slot. The second picture shows the individual cylindrical waves being formed, and the last picture shows the reflected waves still being generated as the flow is being established out through the slot, after the incident shock wave has traveled beyond the field of vision. Fig. 30 is a Schlieren picture of the slot after the outward flow has been established. The wave pattern within this stream of air is typical of underexpanded compressible flow.

VII. Summary of Results and Recommendations

Summary of Results

It was found from this experimental investigation that:

1) In the range of the pressure ratios investigated, the attenuation of the shock wave in passing over the perforated wall was not a function of the pressure ratio, P_{21}.

2) The strength of the incident shock wave after passing over a disturbance (or perforated wall) parallel to the flow is a function of the distance traveled, and therefore the time elapsed.

3) The strength of the incident shock wave after passing over a perforated wall is dependent upon the ease with which the quasi-steady mass flow out through the perforations is established, due to the following two effects:

a) Cylindrical reflected shock waves, which coalesce with and strengthen the incident shock wave, are generated at the hole openings immediately after shock wave passage and during the transition period, or time lag, before a quasi-steady mass flow out through the holes is achieved.

b) Once the quasi-steady flow out through the holes has been established, the resultant loss of mass from behind the incident shock wave generates the rarefaction waves which then weaken the incident shock wave.

As a result of these two effects, for a given open area, a series of many small holes will, at first, only slightly weaken or perhaps even strengthen, momentarily, the incident shock wave; but a series with a few large holes will greatly attenuate the incident shock wave, because the quasi-steady mass flow is established out through the larger holes after a shorter time lag.

4) The strength of the incident shock wave is affected by the rate of the mass flow drawn in through the holes. Two probable effects are possible:

a) The flow of air in through the perforations increases the afore-mentioned time lag before the quasi-steady flow can be established out through the perforations.

b) If the flow rate in through the perforations is high enough, the viscous effects of this flow will decrease $\dot{m}$, the flow associated with the incident shock wave, and weaken it with the resulting generation of expansion waves.

5) The attenuation of the shock wave is a function of the open area per plate, but this function is not linear.

6) The orientation of the incident shock wave is affected by the perforated plates. The cylindrical reflected shock waves, generated at the hole openings, coalesce with and accelerate the incident shock wave. The disturbed portion of the shock wave remains normal to the flow, but the undisturbed portion, which is traveling slower, lags behind at a trailing angle until the

cylindrical wave envelopes the entire incident shock wave and the velocity is once again constant across the face of the wave front. At this time, the entire shock wave is once again normal to the flow.

Recommendations

In order to fully investigate this phenomenon and possibly arrive at a useable mathematical model, it is recommended that:

1) A Schlieren or interferometer study be made of the effects in a channel, at right angles to the shock tube, after shock wave passage.

2) A study of shock interaction be made using high velocity, high pressure air in through the perforations normal to the flow and at different angles of incidence.

VIII. Bibliography

1. Crichton, T.P. The Effect of Tube Length and Diameter on the Pressure Response of Recessed Piezoelectric Transducers. Master's Thesis, Air Force Institute of Technology, September 1959.

2. Dannenberg, R. E., B. I. Gombucci, and J.A. Weiberg. Perforated Sheets as a Porus Material for Distributed Suction and Injection. Technical Note 3669, National Advisory Committee for Aeronautics, April 1956.

3. Davis, Hubert P. and W.A. French. Design and Construction of a Shock Tube. Master's Thesis, Air Force Institute of Technology, August 1955.

4. Diedericks, H. and W.C. Andae. Experimental Mechanical Engineering. Vol I. N.Y.: John Wiley and Sons, 1946.

5. Donaldson, C. and R.D. Sullivan. The Effect of Wall Friction on the Strength of Shock Waves in Tubes and Hydraulic Jumps. Technical Note 1942, National Advisory Committee for Aeronautics 1949.

6. Foy, J.L. Investigation of the Interaction Between a Shock Wave and a Deflagration Wave in a Flowing Hydrogen-Oxygen Nitrogen Mixture. Master's Thesis, Air Force Institute of Technology, August 1959.

7. Glass, I.I. Theory and Performance of Simple Shock Tubes. UTIA Review No.12, Part I, Institute of Aerophysics, University of Toronto, Canada, May 1958.

8. Hall, J.G. Production of Strong Shock Waves; Shock Tube Applications, Design and Instrumentation. UTIA Review No. 12 Part II, Institute of Aerophysics, University of Toronto, Canada, May 1958.

9. Huber, Paul W. and D.R. McFarland. Boundary Layer Growth and Shock Attenuation in a Shock Tube Witn Roughness. Technical Note 3627, National Advisory Committee for Aeronautics, 1956.

10. Masson, D.J. and C. Gazelt Jr. Surface Protection for High Speed Flight. Rand Corp. April 1956.

11. Rudinger, George. The Reflection of Shock Waves From an Orifice at the End of a Duct. Technical Report No. CAL-73-P, Cornell University, 1956.

12. Shapiro, Ascher H. The Dynamics and Thermodynamics of Compressed Fluid Flow. Vol II. N.Y.: The Ronald Press Co. 1954.

13. Sleator, D.B. and M.R. Lewis. A Direct Method of Measuring Density Behind Shock Waves. Report No. 1087, Ballistic Research Laboratories, December 1959.

14. Sun, T.F. On the Attenuation of a Shock From a Slotted Wall. Cornell Aeronautical Laboratories Inc. August 1953.

15. Young, Allen E., Stuart McCullough, and Richard Smith. Power Unit for a High-Intensity Light Source. RM-E-50K27, National Advisory Committee for Aeronautics, July 1951.

Table I
Transducer No. 15 Calibration

Run	M_s	P_{21}	P_1 psia	$P_2 - P_1$ psia	Volts
1.	1.28	1.75	14.57	10.93	.472
2.	1.30	1.75	14.57	11.53	.484
3.	1.33	1.79	14.57	12.73	.524
4.	1.28	1.87	14.57	11.10	.454
5.	1.20	1.76	14.57	7.63	.322
6.	1.18	1.53	14.57	6.63	.276
7.	1.20	1.45	14.57	7.70	.308
8.	1.17	1.53	14.57	6.33	.258
9.	1.12	1.44	14.57	4.31	.164
10.	1.24	1.30	14.57	9.10	.388
11.	1.25	1.62	14.57	9.53	.416
12.	1.21	1.56	14.57	8.13	.338
13.	1.21	1.56	14.57	8.13	.334
18.	1.32	1.87	14.35	12.45	.542
19.	1.32	1.88	14.39	13.61	.605
20.	1.39	2.09	14.39	15.71	.670
21.	1.41	2.17	14.39	16.81	.730
22.	1.17	1.44	14.39	6.31	.284
23.	1.13	1.33	14.39	4.76	.224
24.	1.09	1.23	14.39	3.24	.180
25.	1.20	1.52	14.39	7.41	.338
26.	1.25	1.66	14.39	10.41	.436
27.	1.18	1.48	14.39	6.91	.316
28.	1.26	1.69	14.39	9.91	.430

Table II
Transducer No. 16 Calibration

Run	M_s	P_{21}	p_1 psia	$p_2 - p_1$ psia	Volts
1.	1.28	1.75	14.57	10.93	.464
2.	1.30	1.75	14.57	11.53	.476
3.	1.33	1.79	14.57	12.73	.534
4.	1.28	1.87	14.57	11.10	.452
5.	1.20	1.76	14.57	7.63	.324
6.	1.18	1.53	14.57	6.63	.276
7.	1.20	1.45	14.57	7.70	.304
8.	1.17	1.53	14.57	6.33	.262
9.	1.12	1.44	14.57	4.31	.162
10.	1.24	1.30	14.57	9.10	.384
11.	1.25	1.62	14.57	9.53	.404
12.	1.21	1.56	14.57	8.13	.336
13.	1.21	1.56	14.57	8.13	.334
14.	1.24	1.65	14.35	9.30	.418
15.	1.27	1.73	14.35	10.45	.448
16.	1.29	1.78	14.35	11.15	.490
17.	1.30	1.81	14.35	11.55	.502
18.	1.32	1.87	14.35	12.45	.532
19.	1.32	1.98	14.39	13.61	.600
20.	1.39	2.09	14.39	15.71	.685
21.	1.41	2.17	14.39	16.81	.725
22.	1.17	1.44	14.39	6.31	.284
23.	1.13	1.33	14.39	4.76	.228
24.	1.09	1.23	14.39	3.24	.176
25.	1.20	1.52	14.39	7.41	.340
26.	1.25	1.66	14.39	10.41	.422
27.	1.18	1.48	14.39	6.91	.310
28.	1.26	1.69	14.39	9.91	.430

Table III
Transducer No. 18 Calibration

Run	M_s	P_{21}	p_1 psia	$p_2 - p_1$ psia	Volts
29.	1.32	1.89	14.20	12.7	.486
30.	1.33	1.90	14.20	12.8	.492
31.	1.34	1.94	14.20	13.3	.496
32.	1.28	1.77	14.20	10.9	.430
33.	1.26	1.71	14.20	10.0	.380
34.	1.25	1.69	14.20	9.9	.404
35.	1.27	1.72	14.20	10.2	.376
36.	1.24	1.64	14.20	9.1	.338
37.	1.21	1.56	14.20	7.9	.316
38.	1.20	1.52	14.20	7.3	.278
39.	1.19	1.48	14.20	6.9	.256
40.	1.25	1.68	14.20	9.7	.276
41.	1.30	1.81	14.20	11.4	.420
42.	1.33	1.90	14.20	12.8	.484
43.	1.35	1.95	14.20	13.5	.530
44.	1.35	1.95	14.20	13.5	.528
45.	1.39	2.08	14.20	15.4	.592
46.	1.42	2.15	14.20	16.3	.646

Table IV

Attenuation Between Stations C and D

Run	p_1	$(p_2-p_1)_C$	p_{2C}	$(p_1-p_2)_D$	p_{2D}	P_{21C}	P_{21D}	Z_D
	psia.	psia.	psia.	psia.	psia.			%
47.	14.30	11.2	25.50	11.3	25.60	1.782	1.792	-1.3
48.	14.30	12.4	26.70	.2.2	26.60	1.869	1.859	+1.1
49.	14.30	13.1	27.40	13.0	27.30	1.916	1.909	+0.7
50.	14.30	12.7	27.00	12.8	27.10	1.889	1.894	-0.6
51.	14.30	10.8	25.10	10.8	25.10	1.755	1.755	0
52.	14.30	9.8	24.10	9.7	24.00	1.687	1.678	+1.3
53.	14.30	11.4	25.70	11.6	25.90	1.798	1.811	-1.6
54.	14.30	11.1	25.40	11.1	25.40	1.778	1.778	0
55.	14.30	11.3	25.60	11.2	25.50	1.791	1.731	+1.3
56.	14.30	12.1	26.40	12.0	26.30	1.847	1.839	+0.9
							Average	+1.1

Table V

Attenuation Between Stations C and E

Run	p_1	$(p_2-p_1)_C$	p_{2C}	$(p_1-p_2)_E$	p_{2D}	P_{21C}	P_{21E}	Z_E
	psia.	psia.	psia.	psia.	psia.			%
57.	14.34	10.0	24.31	9.2	23.54	1.693	1.641	+7.5
58.	14.34	12.9	27.24	12.2	26.54	1.900	1.851	6.5
59.	14.34	13.4	27.74	12.5	26.84	1.932	1.872	6.4
60.	14.34	13.6	27.94	12.6	26.94	1.948	1.879	7.3
61.	14.34	11.4	25.74	10.7	25.04	1.794	1.748	5.8
62.	14.34	11.2	25.54	10.4	24.74	1.781	1.724	7.3
63.	14.34	11.6	25.94	10.9	24.24	1.809	1.761	5.9
64.	14.34	10.8	25.14	10.0	24.34	1.753	1.697	7.4
65.	14.34	11.2	25.54	10.6	24.94	1.781	1.739	5.4
66.	14.34	12.2	26.54	11.3	25.64	1.851	1.789	7.3
							Average	+6.7

Table VI

Attenuation From a 0.125 Inch Slot

0.491 $in.^2$ Open Area Per Plate

Run	Flow lbs/sec	P_{21C}	P_{21D}	P_{21E}	Z_D %	Z_E %
67.	0	1.740	1.678	-	+8.4	-
68.	0	1.458	1.387	-	15.5	-
69.	0	1.421	1.374	-	11.1	-
70.	0	1.815	1.706	-	13.4	-
71.	0	1.920	1.810	-	11.9	-
72.	0	1.961	1.851	-	12.9	-
73.	0	2.055	1.920	-	12.8	-
74.	0	2.142	2.010	-	11.6	-
75.	0	1.421	-	1.285	-	+32.3
76.	0	1.387	-	1.318	-	20.2
77.	0	1.740	-	1.554	-	25.2
78.	0	1.970	-	1.727	-	25.1
79.	.0217	1.987	1.829	-	16.2	-
80.	.0217	2.188	2.009	-	14.6	-
81.	.0217	1.498	1.433	-	13.1	-
82.	.0217	2.060	1.908	-	14.4	-
83.	.0217	1.771	-	1.555	-	28.1
84.	.0217	1.621	-	1.454	-	26.9
85.	0	2.107	1.983	1.864	11.2	21.9
86.	0	2.198	2.067	1.899	10.9	25.1
87.	0	2.310	2.187	1.962	9.4	26.6
88.	.0217	2.250	2.069	1.878	14.5	29.6
89.	.0217	2.030	1.849	1.747	17.6	27.5
90.	.0217	1.504	1.425	1.388	18.6	23.1
91.	.0217	2.245	2.069	1.900	14.2	27.7
92.	.0217	2.398	2.193	1.981	14.7	29.9

Table VII

Attenuation From 40-0.125 Inch Holes Per Plate
0.491 $in.^2$ Open Area

Run	Flow lbs/sec	P_{21C}	P_{21D}	P_{21E}	Z_D %	Z_E %
93.	0	1.665	1.645	-	+3.0	-
94.	0	1.383	1.384	-	0	-
95.	0	1.790	1.762	-	+3.5	-
96.	0	2.002	2.002	-	0	-
97.	0	2.105	2.105	-	0	-
98.	0	1.901	1.901	-	0	-
99.	0	1.333	1.319	-	+5.1	-
100.	0	2.325	2.278	-	+3.5	-
101.	0	2.220	2.220	-	0	-
102.	0	2.095	-	1.970	-	+11.4
103.	0	1.860	-	1.767	-	+10.8
104.	0	2.150	-	1.980	-	+14.7
105.	0	2.150	-	1.997	-	+13.3
106.	.0217	1.763	-	1.650	-	+14.8
107.	.0217	1.915	-	1.793	-	+13.4
108.	.0217	2.283	-	2.115	-	+13.1
109.	.0217	1.755	-	1.665	-	+11.9
110.	.0217	2.225	-	2.055	-	+13.8
111.	.0217	2.330	-	2.170	-	+12.0
112.	.0217	2.395	-	2.212	-	+13.1
113.	.0217	1.720	1.701	-	+1.8	-
114.	.0217	1.625	1.650	-	-4.0	-
115.	.0217	1.793	1.820	-	-3.4	-
116.	.0217	2.000	2.080	-	-8.0	-
117.	.0217	2.100	2.200	-	-9.1	-
118.	.0217	2.127	2.230	-	-8.6	-
119.	.0217	2.30	2.350	-	-9.8	-
120.	.0217	2.280	2.360	-	-6.3	-
121.	.0217	2.315	2.385	-	-5.3	-
122.	0	1.905	-	1.791	-	+12.6
123.	0	1.709	-	1.602	-	+15.1
124.	0	2.193	-	2.052	-	+11.8
125.	0	1.661	-	1.581	-	+12.1

Table VIII

Attenuation Form 80-0.125 Inch Holes Per Plate

(0.982 in^2 Open Area)

Run	Flow lbs/sec	P_{21C}	P_{21D}	Z_D %
126.	0	1.862	1.955	-10.5
127.	0	1.764	1.847	-10.9
128.	0	1.793	1.903	-12.6
129.	0	1.931	2.030	-10.6
130.	0	1.807	1.930	-11.9
131.	0	1.807	1.898	-11.2
132.	0	1.749	1.777	- 3.7
133.	0	1.582	1.609	- 4.6
134.	0	1.534	1.539	- 0.9
135.	.0217	1.920	2.033	-12.3
136.	.0217	1.976	2.133	-16.1
137.	.0217	2.075	2.223	-13.7
138.	.0217	2.033	2.217	-17.8
139.	.0217	1.733	1.862	-17.9
140.	.0217	1.806	1.899	-11.5
141.	.0306	1.950	2.072	-12.9
142.	.0306	1.902	2.015	-12.5
143.	.0306	1.902	2.022	-13.3
144.	.0306	1.815	1.879	- 7.9
145.	.0306	1.643	1.686	- 6.7
146.	.0306	1.637	1.693	- 8.7
147.	.0306	1.508	1.579	-14.1
148.	.0217	1.935	2.047	-12.0
149.	.0217	1.950	2.082	-13.9
150.	.0217	1.962	2.063	-10.5
151.	.0217	1.978	2.063	- 8.7
152.	.0217	1.978	2.042	- 6.5
153.	.0306	1.988	2.067	- 8.0
154.	.0306	1.999	2.087	- 8.8
156.	.0306	1.978	2.095	-11.1
157.	.0306	1.959	2.059	-10.5
158.	.0306	1.992	2.102	-11.1
159.	0	1.953	2.058	-11.0
160.	0	1.903	1.989	- 9.5
161.	0	1.947	2.012	- 5.7
162.	0	1.912	1.958	- 5.1
163.	0	1.973	2.045	- 7.4

Continued:

Table VIII Continued

Run	Flow lbs/sec	P_{21C}	P_{21D}	Z_D %
164.	.0159	1.852	2.023	-20.1
165.	.0159	1.936	2.047	-11.8
166.	.0159	1.908	2.073	-18.2
167.	.0159	1.943	2.083	-14.9
168.	.0159	1.917	2.025	-12.9
169.	.0159	1.943	2.073	-13.8
170.	.0159	1.943	2.086	-15.2
171.	.0159	1.973	2.152	-18.3
172.	.0125	1.960	2.058	-10.2
173.	.0125	1.828	1.853	- 4.3
174.	.0125	1.866	1.938	- 8.3
175.	.0125	1.818	1.938	-14.7
176.	.0125	1.925	1.971	- 5.0
177.	.0125	1.840	1.947	-12.7
178.	.0125	1.953	2.025	- 8.4
179.	.0125	1.973	2.032	- 6.1
180.	.0090	1.960	2.033	- 7.6
181.	.0090	1.918	2.002	- 9.2
182.	.0090	1.941	1.997	- 6.0
183.	.0090	1.918	1.997	- 8.6
184.	.0090	1.927	2.025	-10.5
185.	.0090	1.918	2.013	-10.4
186.	.0375	1.781	1.719	+ 8.9
187.	.0375	1.781	1.723	+ 7.4
188.	.0375	1.730	1.667	+ 8.6
189.	.0375	1.752	1.683	+ 9.2
190.	.0375	1.752	1.683	+ 9.2
191.	.0375	1.779	1.739	+ 5.1
193.	.0375	1.753	1.723	+ 4.0
194.	.0375	1.779	1.739	+ 5.1
195.	.0375	1.730	1.683	+ 6.4
196.	.0374	1.781	1.751	+ 3.8

Table IX
Attenuation From 80-0.125 Inch Holes Per Plate
No Flow

Run	P_{21C}	P_{21E}	Z_E %
197.	1.766	1.653	+14.8
198.	1.836	1.718	+14.1
199.	1.766	1.669	+12.6
200.	1.794	1.704	+11.3
201.	1.800	1.704	+ 9.5
202.	1.766	1.669	+12.6
203.	1.766	1.675	+11.8
204.	1.780	1.674	+13.6
205.	1.808	1.702	+13.1
206.	1.800	1.681	+14.9
		Average	+12.8

Table X

Attenuation From Various Size Holes
For 0.982 $in.^2$ Open Area Per Plate

Run	Hole Size in.	P_{21C}	P_{21D}	Z_D %
207.	.25	1.773	1.773	. 0
208.	"	1.765	1.793	- 3.7
209.	"	1.865	1.904	- 4.5
210.	"	1.918	1.918	0
211.	"	1.888	1.904	- 1.8
212.	"	1.773	1.807	- 4.4
213.	"	1.814	1.832	- 2.2
214.	"	1.779	1.820	- 5.2
215.	.35	1.829	1.722	+12.9
216.	"	1.801	1.735	+ 8.2
217.	"	1.801	1.735	+ 8.2
218.	"	1.792	1.710	+10.3
219.	"	1.808	1.722	+10.6
220.	"	1.843	1.765	+ 9.3
221.	"	1.816	1.739	+ 9.4
222.	"	1.808	1.731	+ 9.5
223.	"	1.808	1.728	+ 9.9
224.	"	1.816	1.734	+10.1
225.	.50	1.721	1.645	+10.5
226.	"	1.807	1.706	+12.5
227.	"	1.771	1.650	+15.7
228.	"	1.791	1.692	+12.5
229.	"	1.807	1.700	+13.3
230.	"	1.771	1.663	+14.0
231.	"	1.843	1.720	+14.6
232.	"	1.791	1.678	+14.3
233.	"	1.800	1.692	+13.5
234.	.25Slot	1.907	1.759	+16.3
235.	"	1.900	1.759	+15.7
236.	"	1.934	1.816	+18.8
237.	"	1.907	1.759	+16.3
238.	"	1.863	1.719	+16.7
239.	"	1.900	1.751	+16.6

Table XI
Attenuation From 20-.25 Inch Holes
Per Plate, Flow
Equals .0217 lbs/sec

Run	P_{21C}	P_{21D}	$Z_{\%D}$
240.	1.809	1.839	-3.7
241.	1.823	1.888	-7.9
242.	1.809	1.831	-2.7
243.	1.819	1.889	-8.6
244.	1.823	1.851	-2.4
245.	1.879	1.917	-4.3
246.	1.847	1.902	-6.5
247.	1.838	1.872	-4.1

Table XII

Attenuation From Different Numbers of
0.50 Inch Holes Per Plate
No Flow

Run	No. 0.50 In. Holes	P_{21C}	P_{21D}	$Z_{\%D}$
248.	3	1.900	1.815	9.4
249	3	1.887	1.815	8.1
250.	3	1.922	1.830	10.0
251.	3	1.915	1.839	8.3
252.	3	1.887	1.802	9.6
253.	10	1.910	1.748	18.9
254.	10	1.901	1.748	17.0
255.	10	1.910	1.757	16.8
256.	10	1.901	1.748	17.0
257.	10	1.910	1.742	18.5
258.	20	1.986	1.769	22.0
259.	20	1.965	1.747	22.6
260.	20	1.971	1.774	20.3
261.	20	1.965	1.747	22.6
262.	20	1.957	1.759	20.7

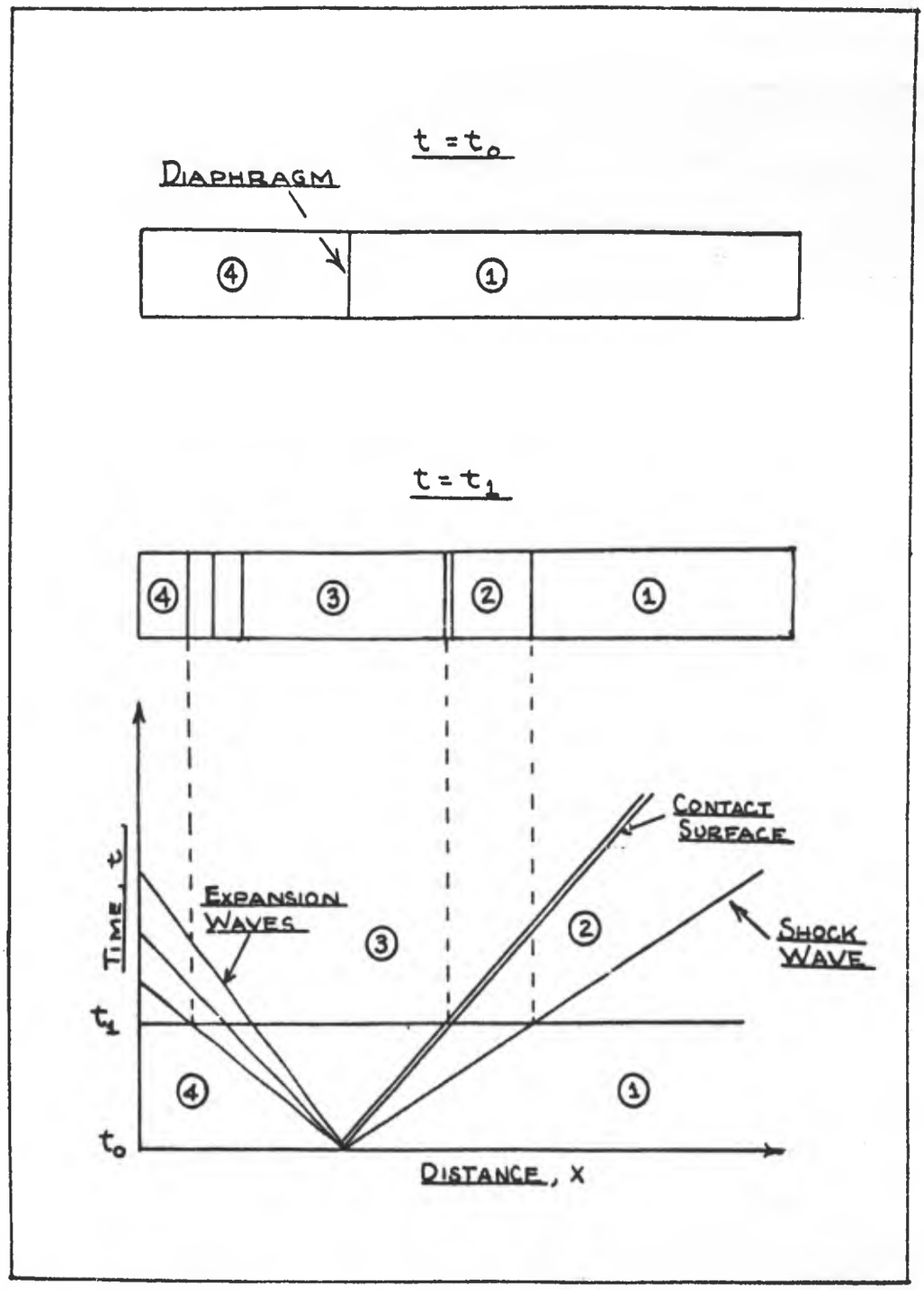

Figure 1. Flow in a Shock Tube

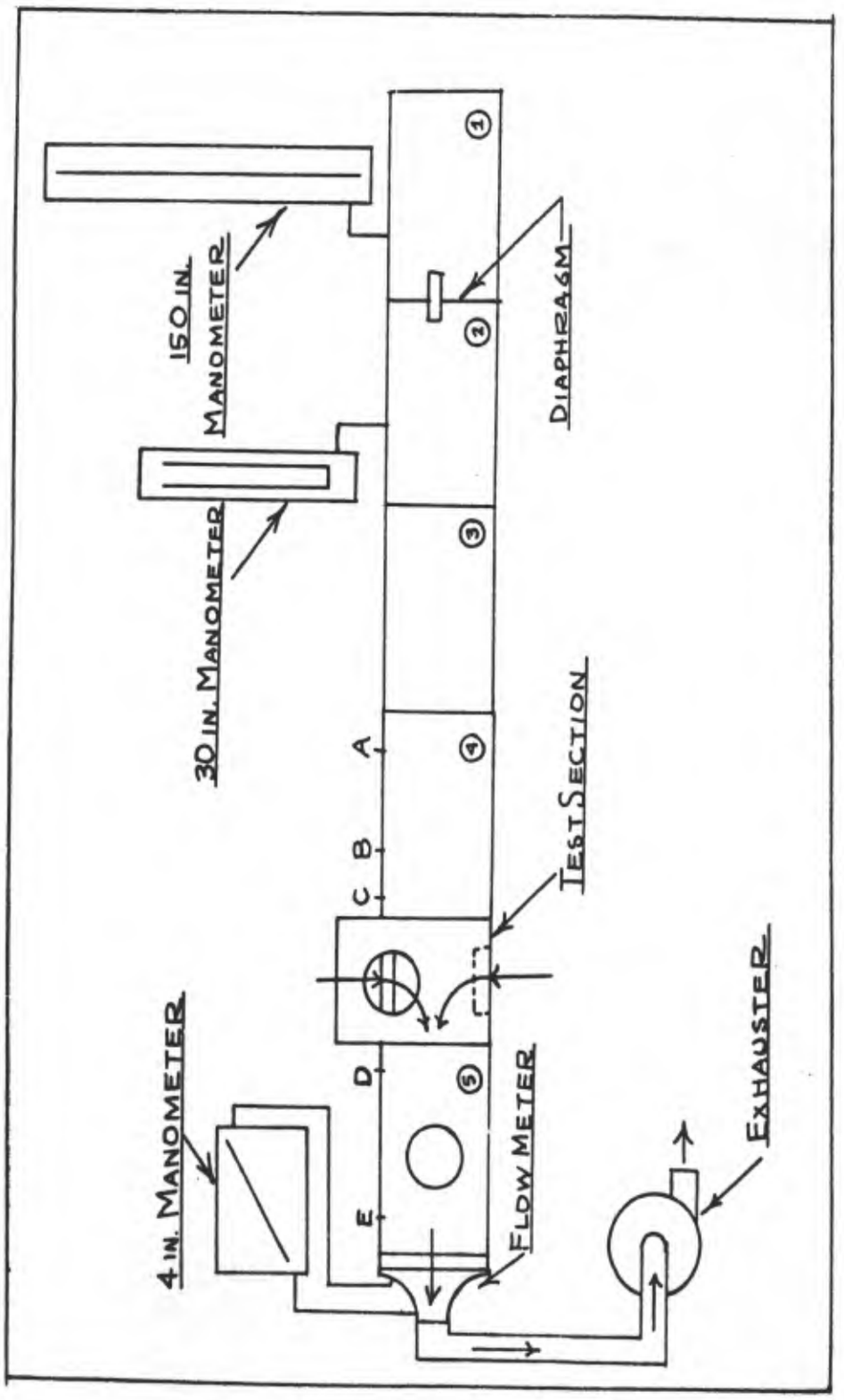

Figure 2. Shock Tube Schematic

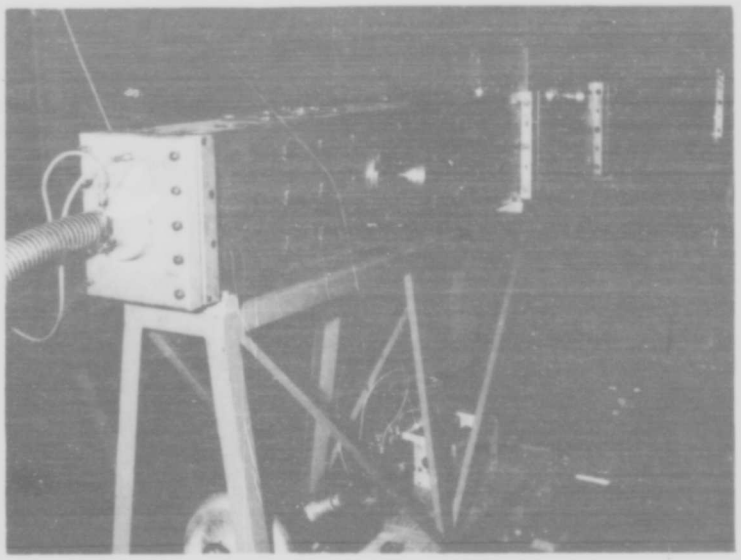

Figure 3. General view of Shock Tube

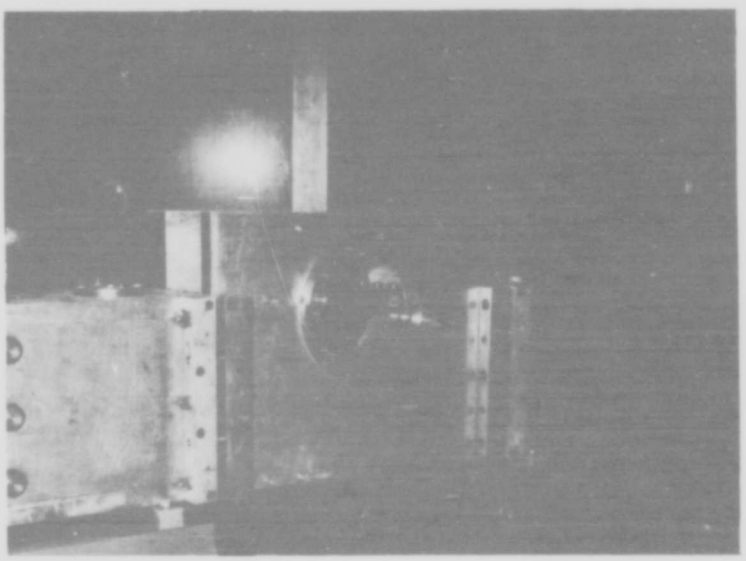

Figure 4. General View of Test Section

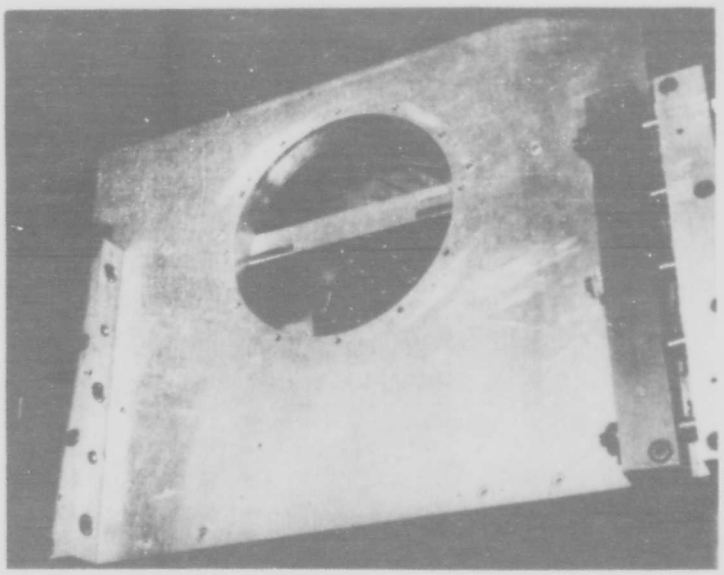

Figure 5. Test Section With Right-hand View-port Removed

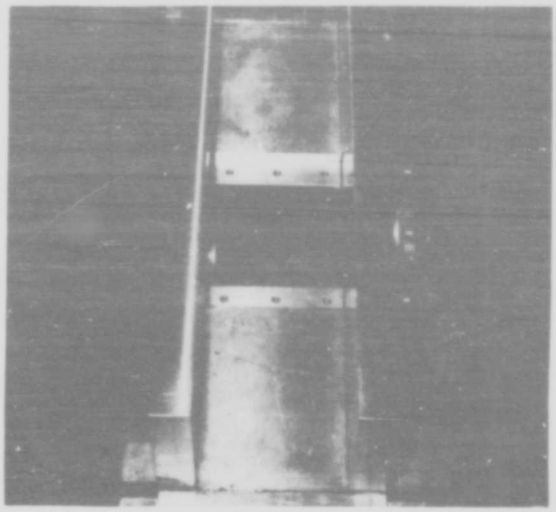

Figure 6. Test Section with Top Plate Removed

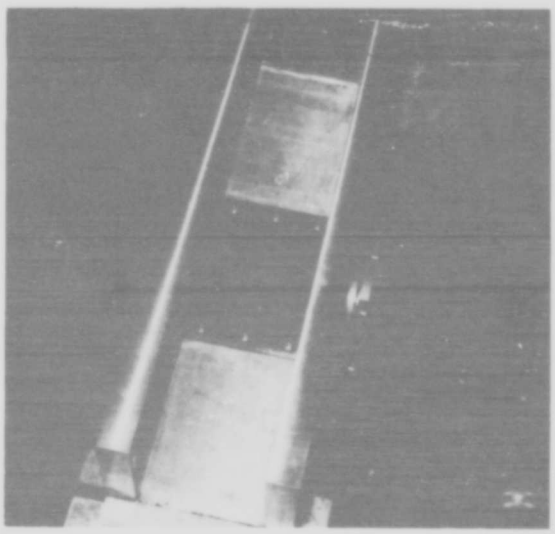

Figure 7. Test Section With Top Plate in Place

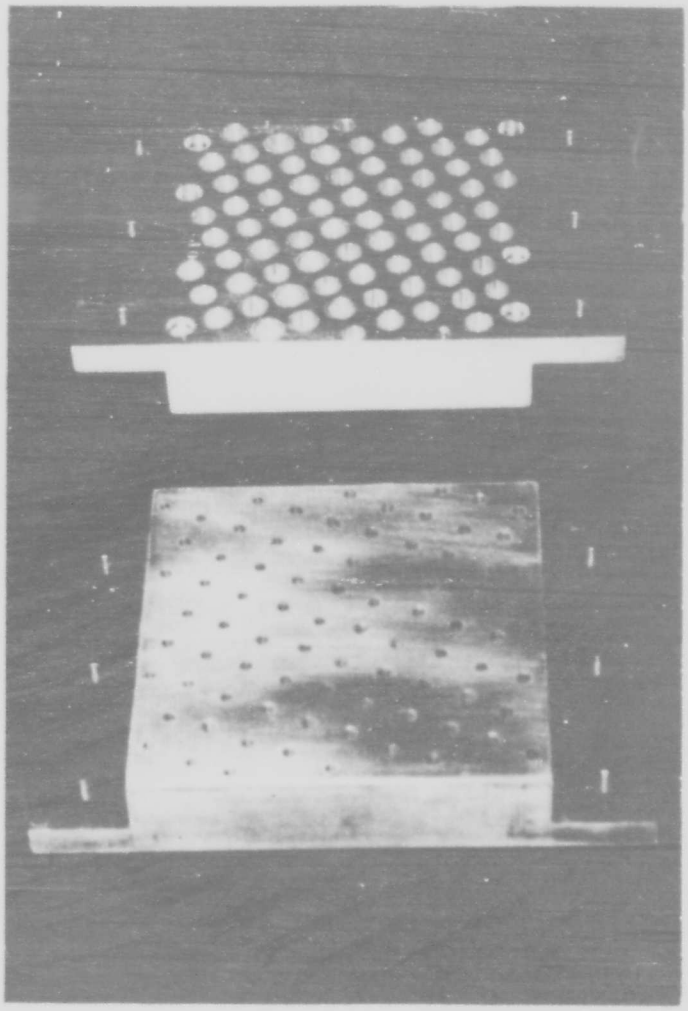

Figure 8. Test Plates With 80-0.125 In. Diameter Holes

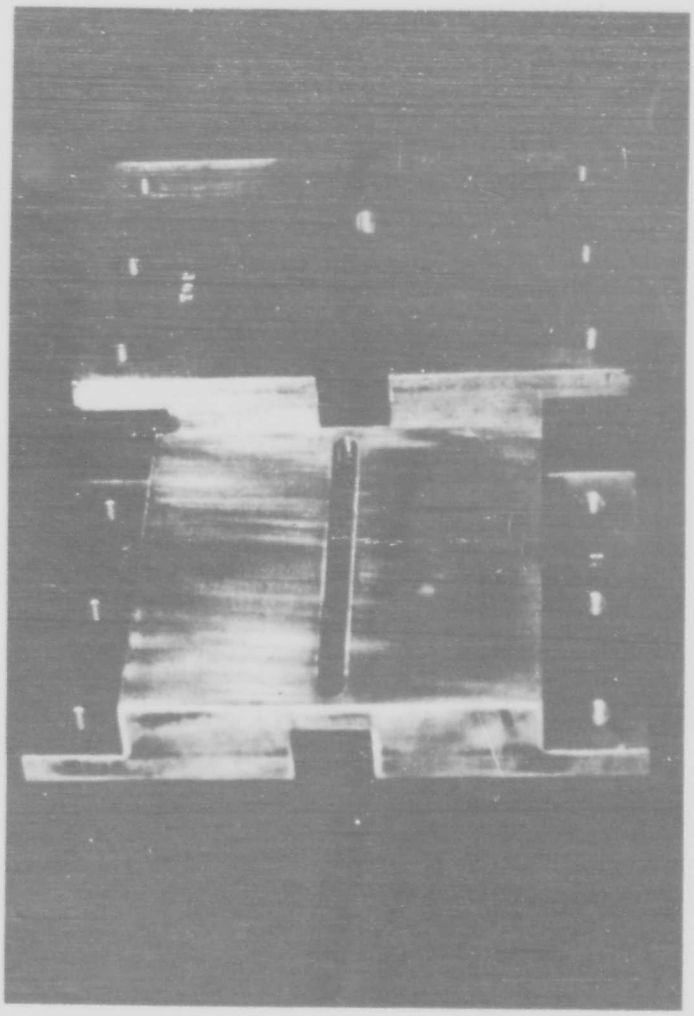

Figure 9. Test Plates With 0.25 In. Slots

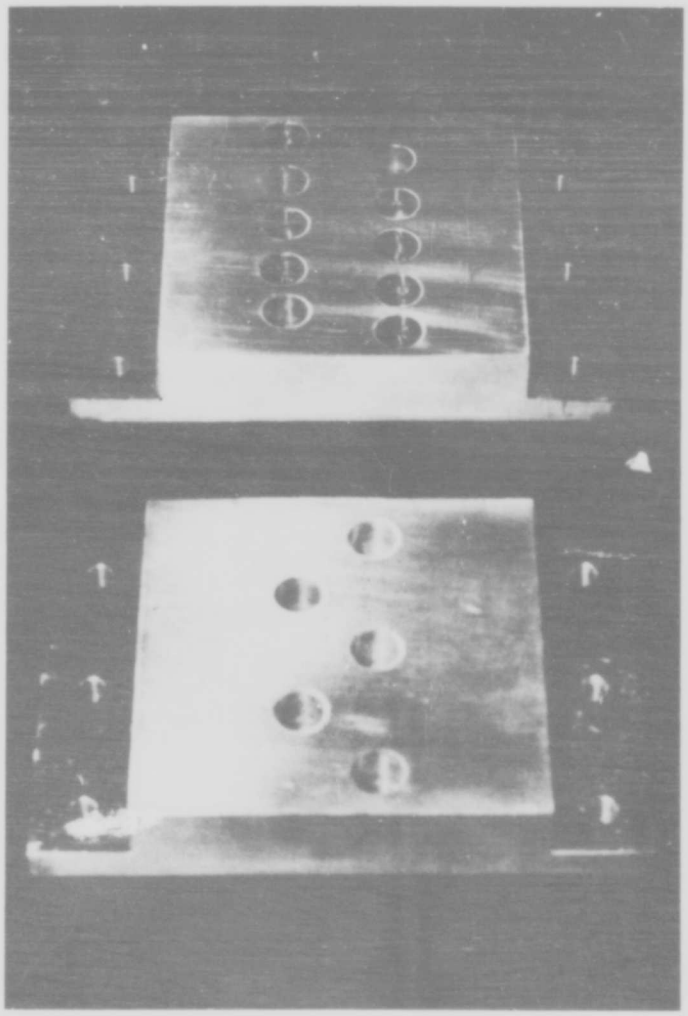

Figure 10. Test Plates With 5 and 10-0.50 In. Diameter Holes

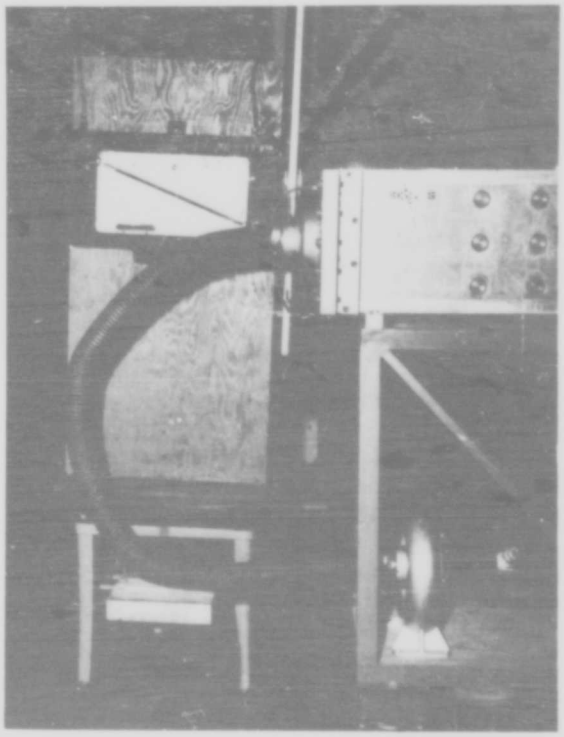

Figure 11. Exhaust System

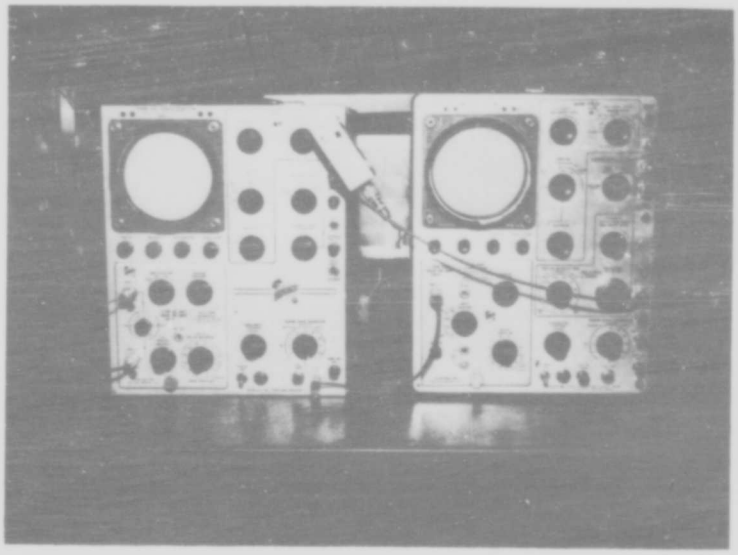

Figure 12. Type 531 and Type 1805 Oscilloscopes

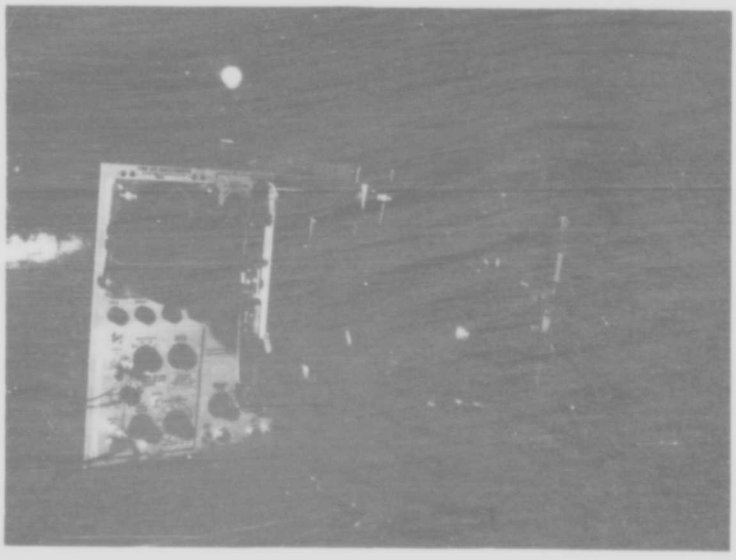

Figure 13. Oscilloscope Cameras Mounted

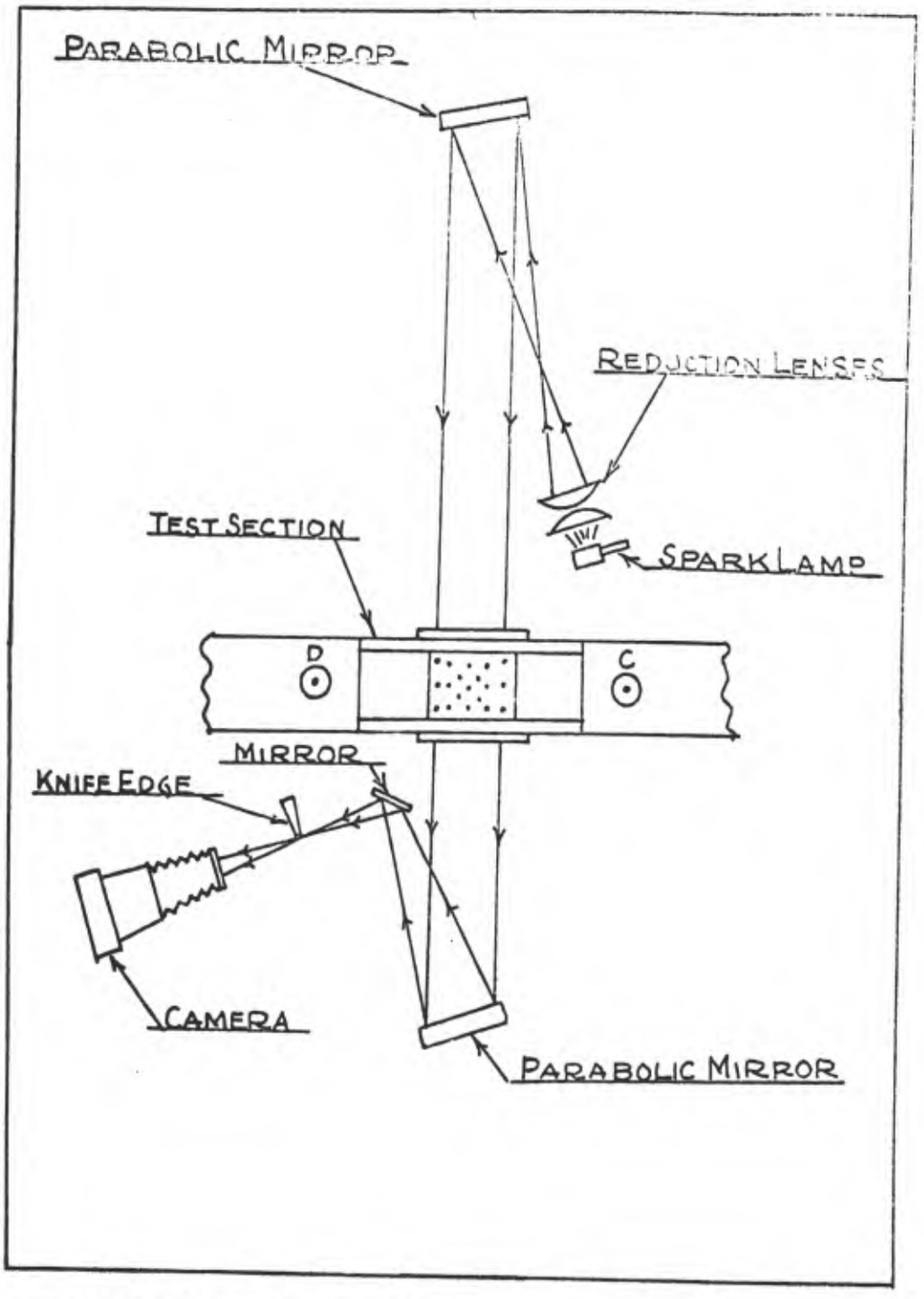

Figure 14. Schlieren Photography Set-up

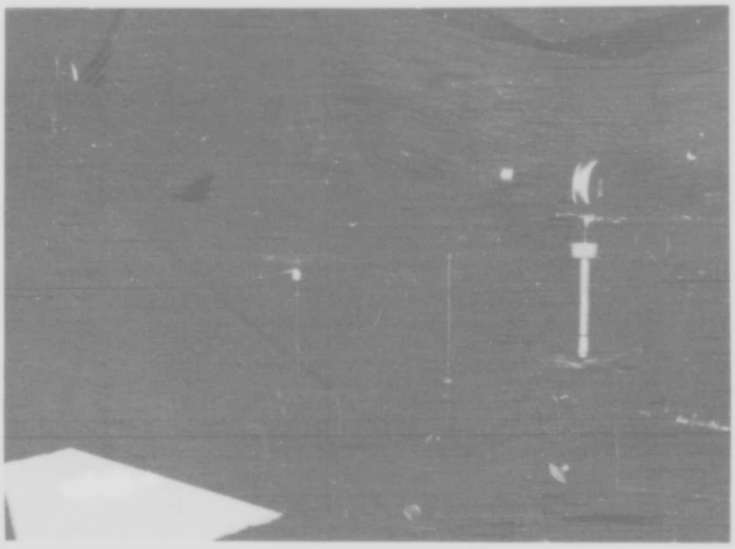

Figure 15. Schlieren Camera, Knife Edge, and Mirror

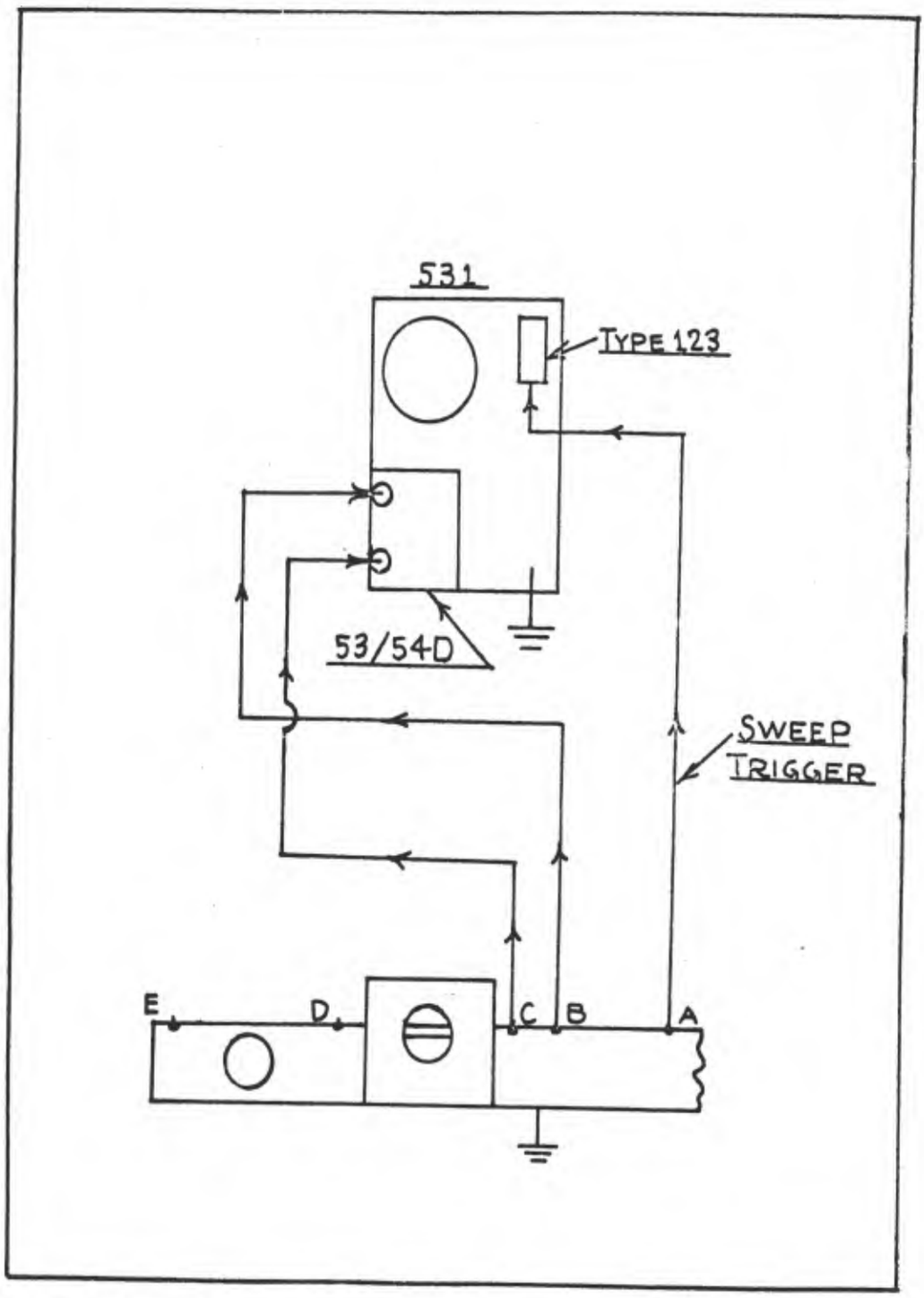

Figure 16. Calibration Electronic Configuration

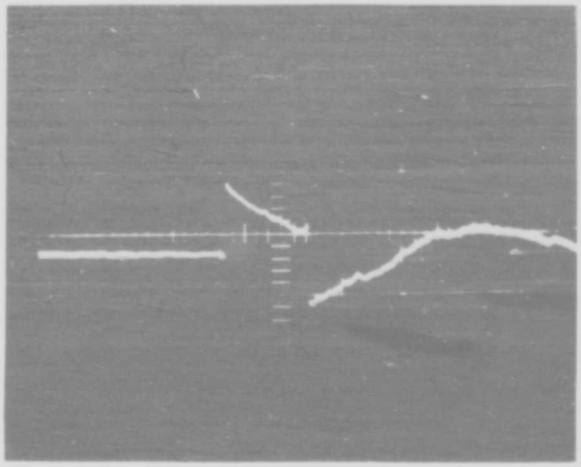

Figure 17. Oscilloscope Picture during Transducer Calibration

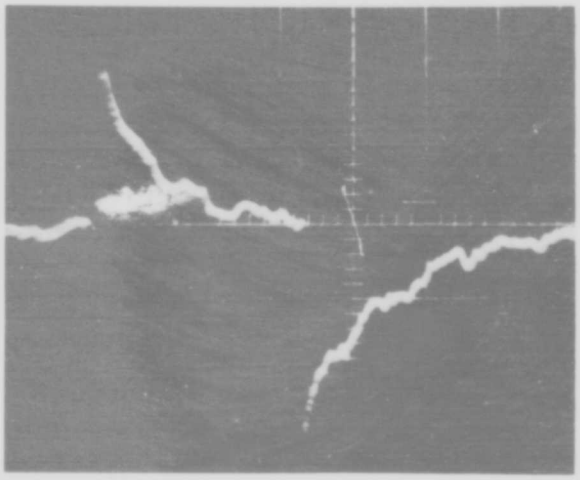

Figure 18. Oscilloscope Picture During Experiment Runs

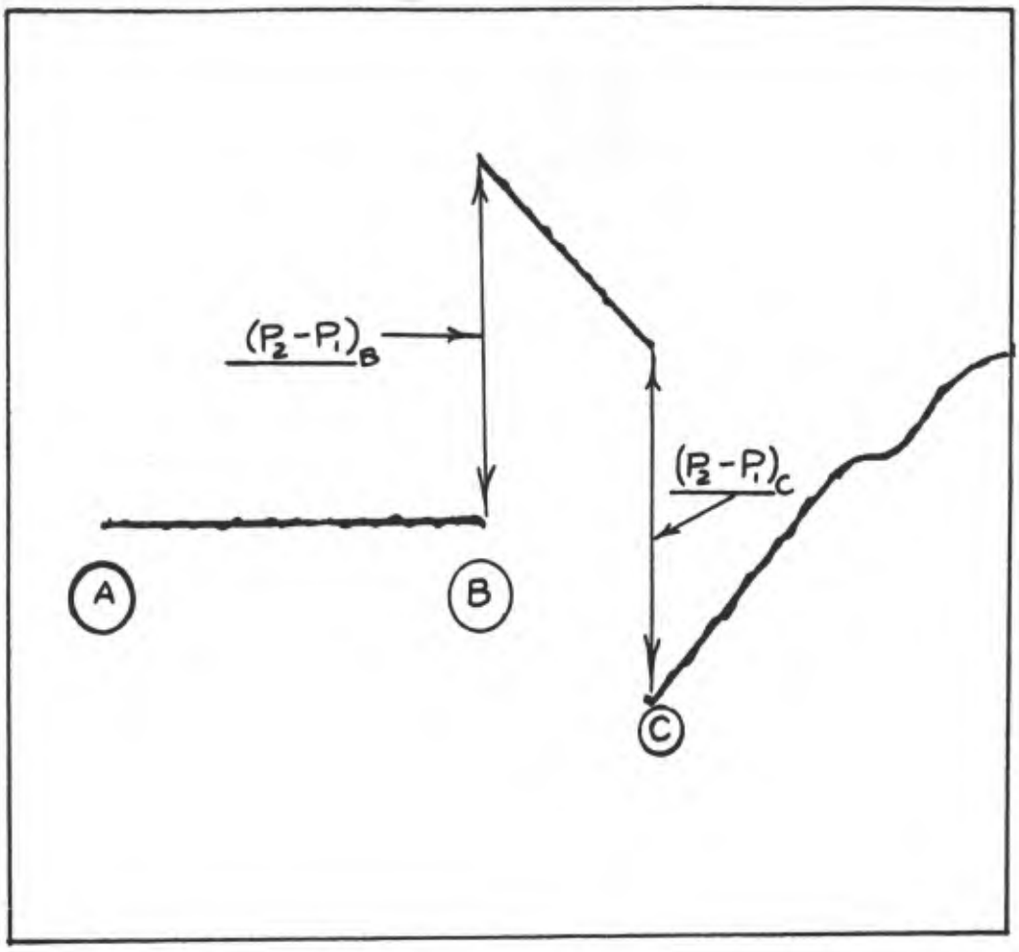

Figure 19. Sketch of Oscilloscope's Trace For Calibration

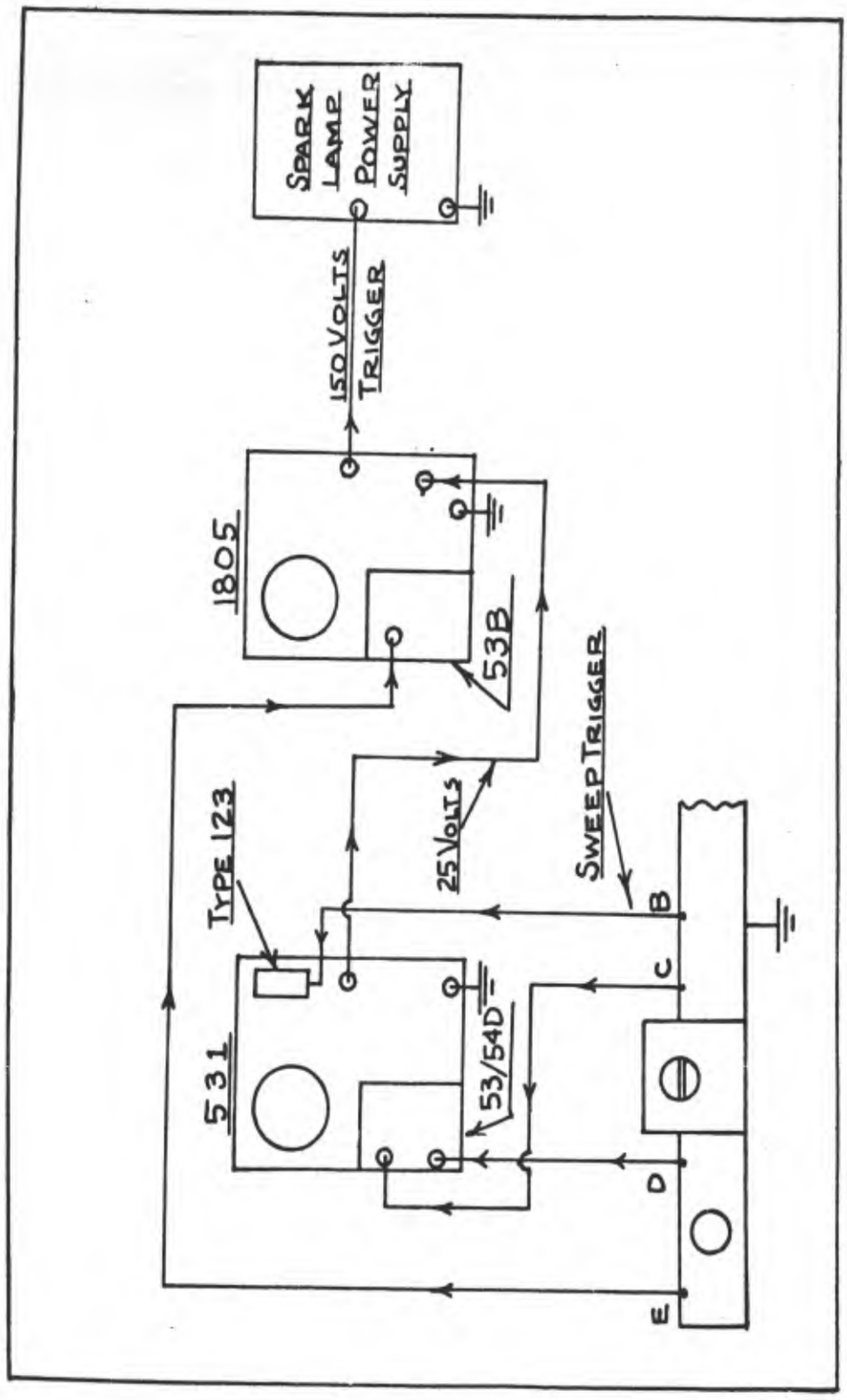

Figure 20. Experimental Electronic Configuration

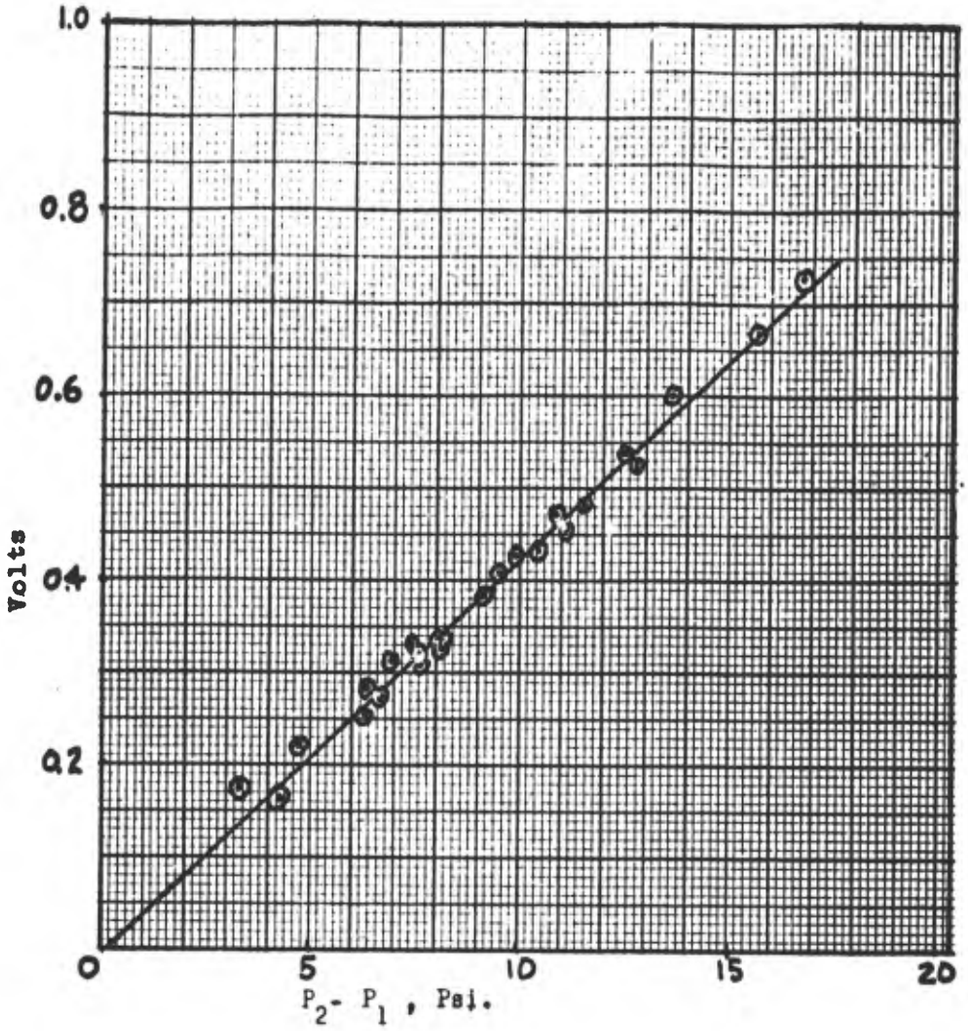

Figure 21. Calibration Curve, Transducer Number 15

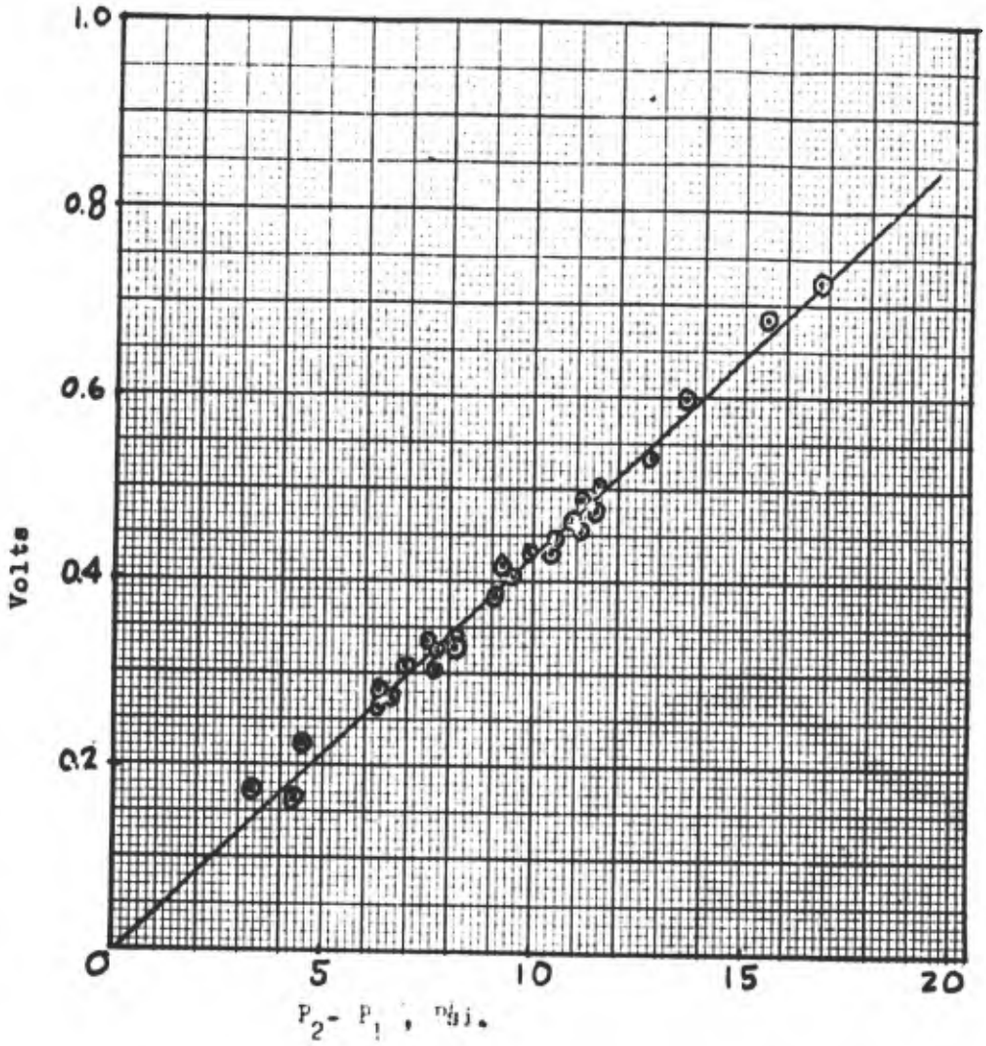

Figure 22. Calibration Curve, Transducer Number 16

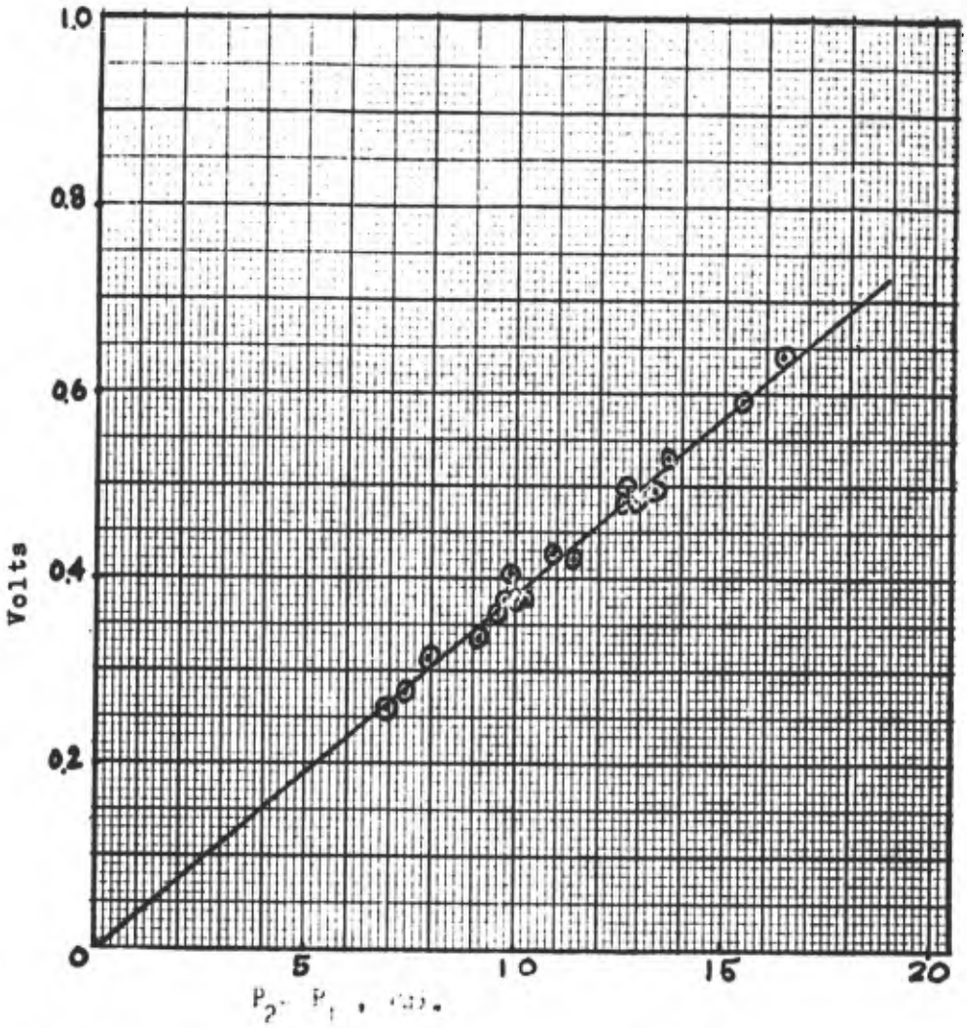

Figure 23. Calibration Curve, Transducer Number 18

Figure 24. Schlieren Photography of a Shock Wave Passing Over Blank Plates.

Figure 25. Schlieren Photography of a Shock Wave Passing Over 80-0.125 In. Diameter Holes, No Flow.

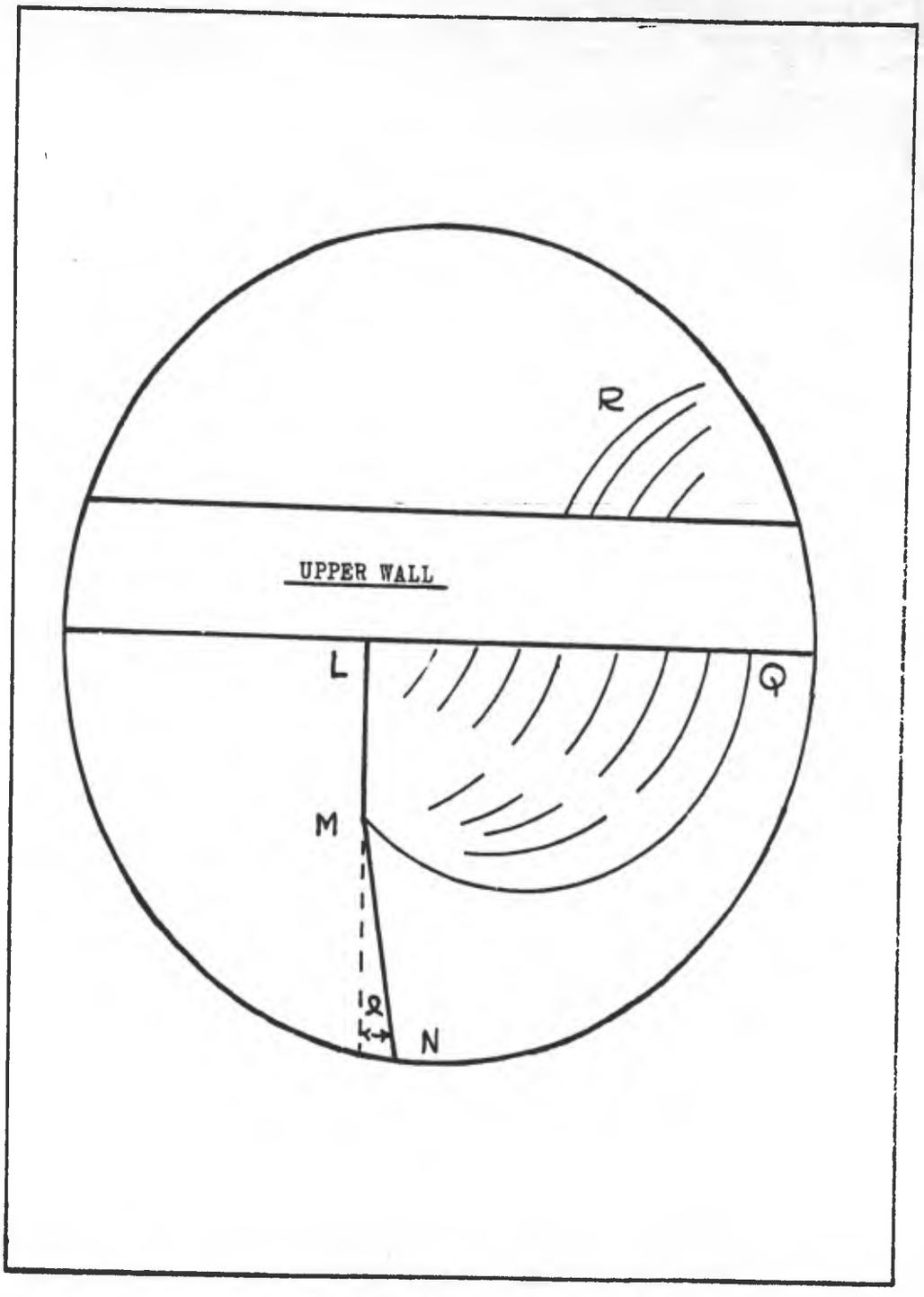

Figure 26. Orientation of Incident Shock Wave As It Passes Over a Perforated Wall

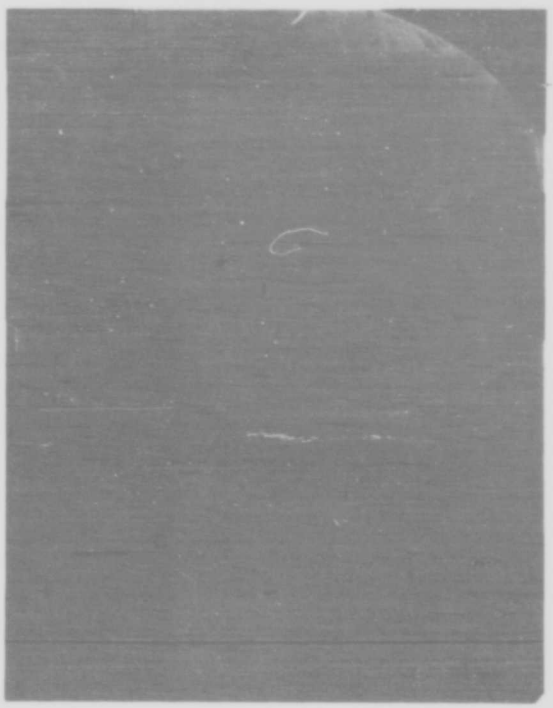

Figure 27. Schlieren Photography of a Shock Passing Over 80-0.125 In. Diameter Holes, Flow=.02171bs/sec.

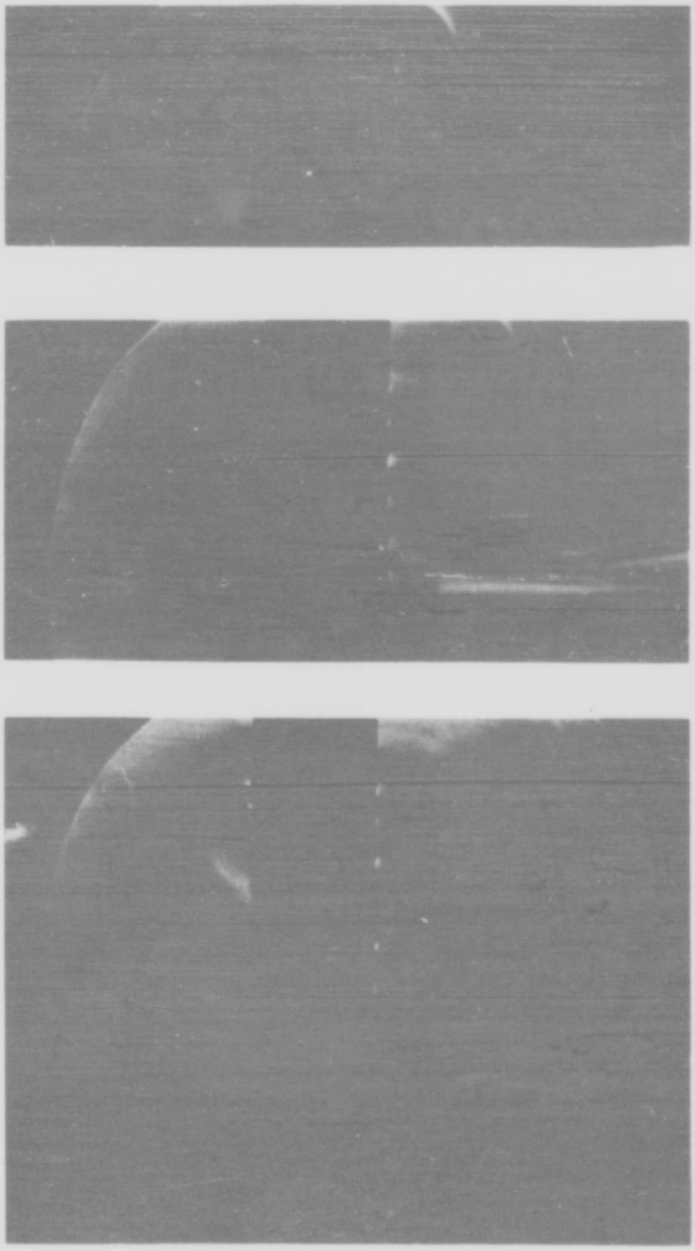

Figure 28. Composite Schlieren Photographs of a Shock Passing Over 20-0.25 In Diameter Holes.

Figure 29. Composite Schlieren Photographs of a Shock Wave Passing Over a 0.25 Inch Slot.

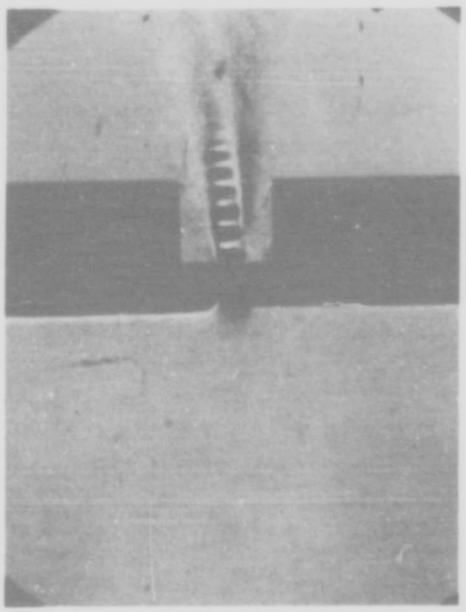

Figure 30. Flow Established Out Through a 0.25 Inch Slot.

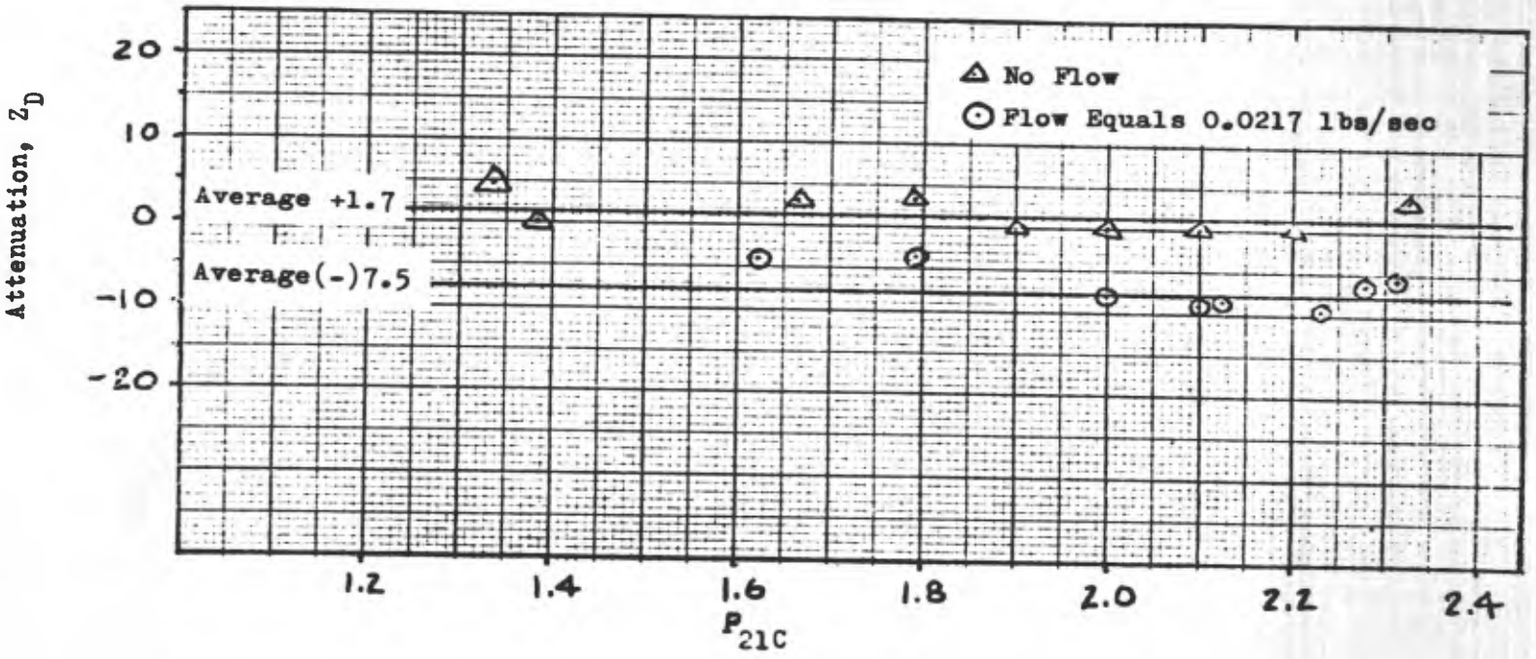

Figure 31. Attenuation Due to 40-0.125in. Diameter Holes Per Plate Measured At Station D (With and Without Flow)

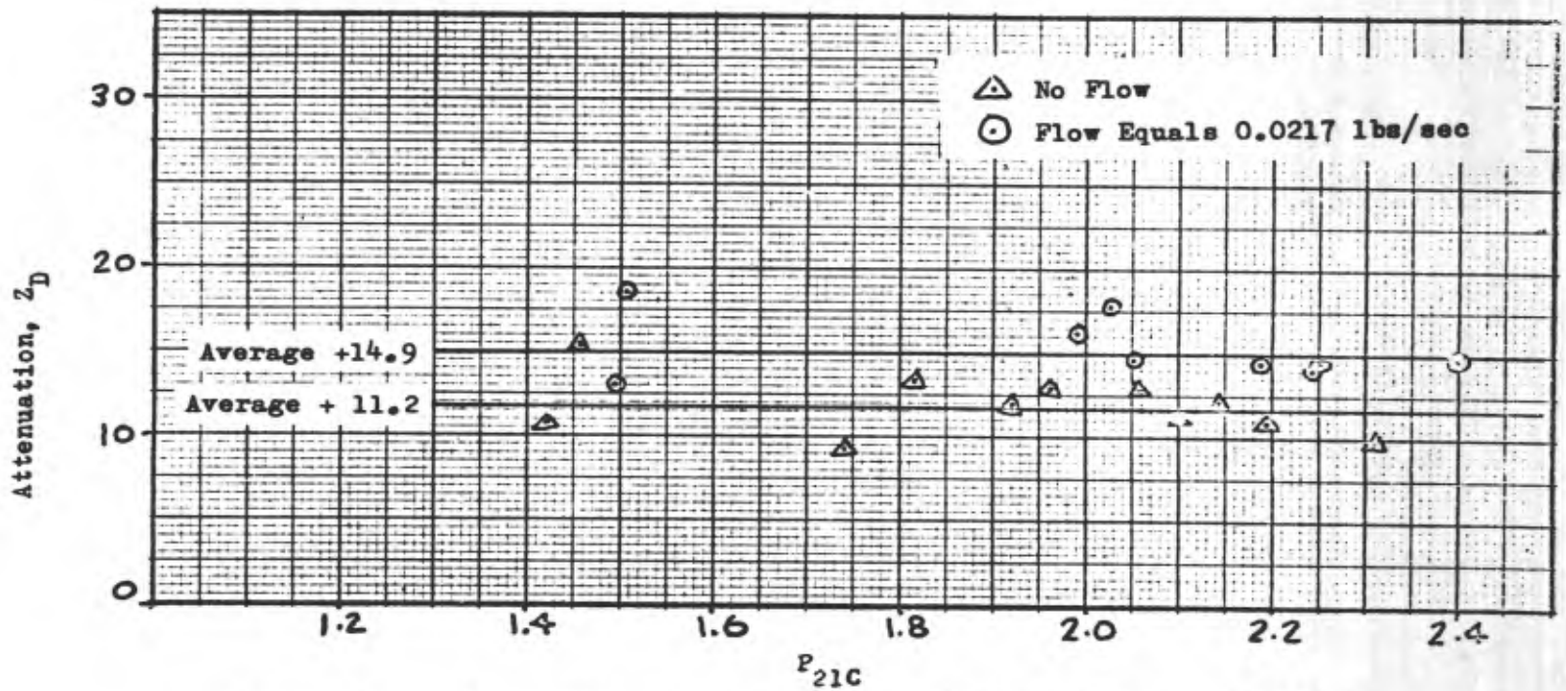

Figure 32. Attenuation Due to 0.125 in. Slot Measured at Station D
(With and Without Flow)

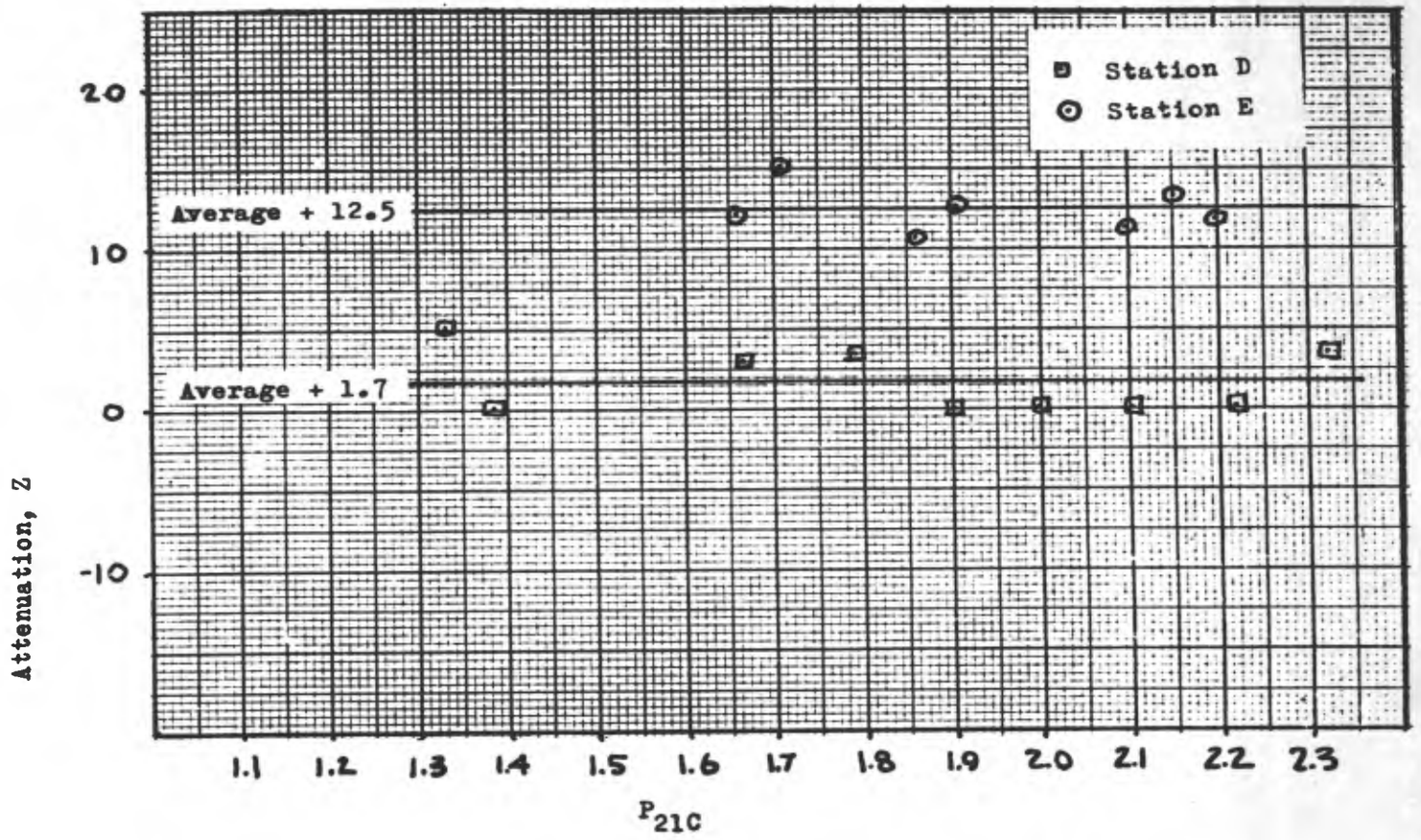

Figure 33. Attenuation Due to 40-0.125Diameter Holes Per Plate Measured at Stations D and E. (No Flow)

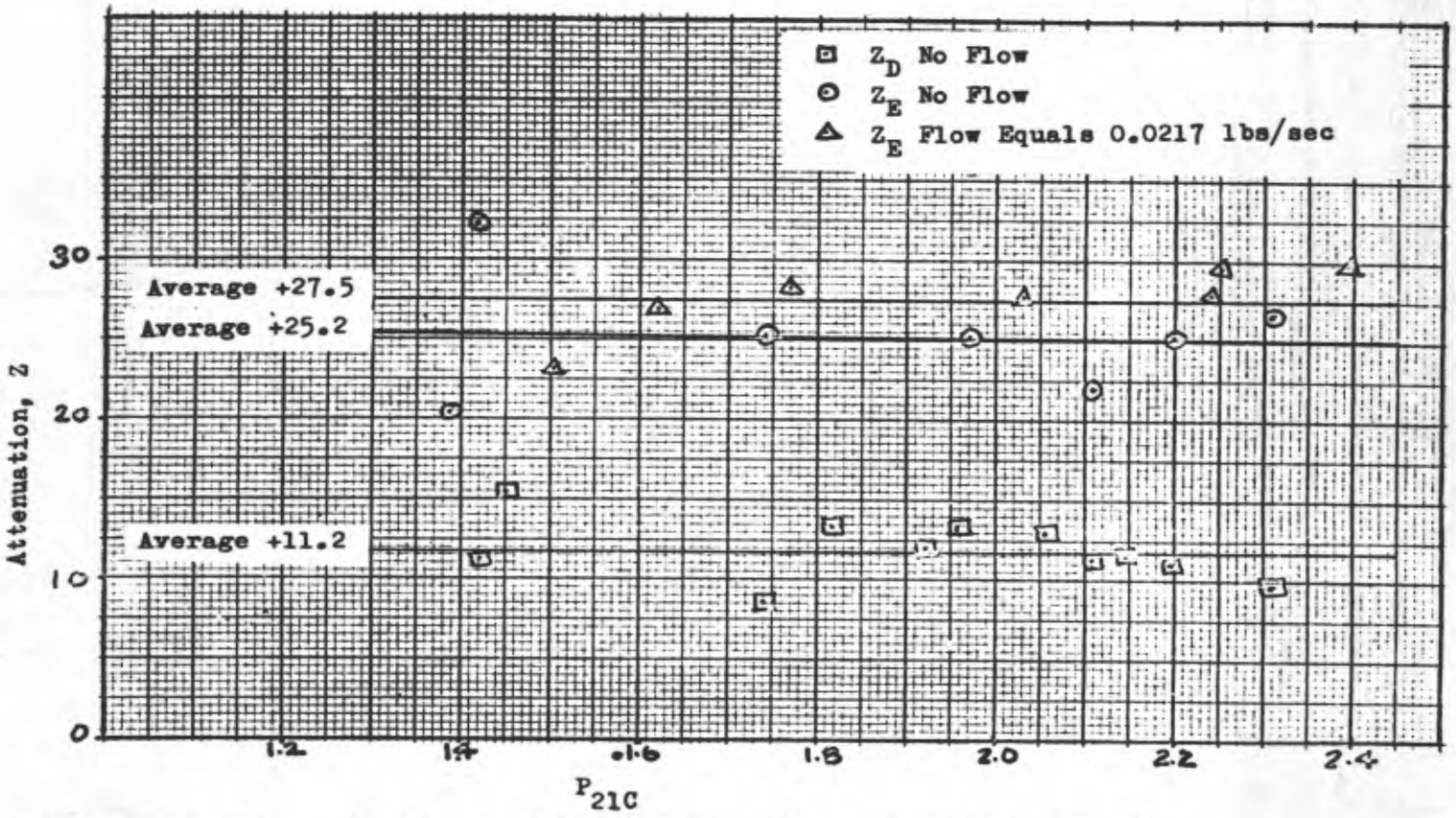

Figure 34. Attenuation Due to 0.125 in. Slot Measured at Station D (Without Flow) Compared to That Measured at Station E (With and Without Flow)

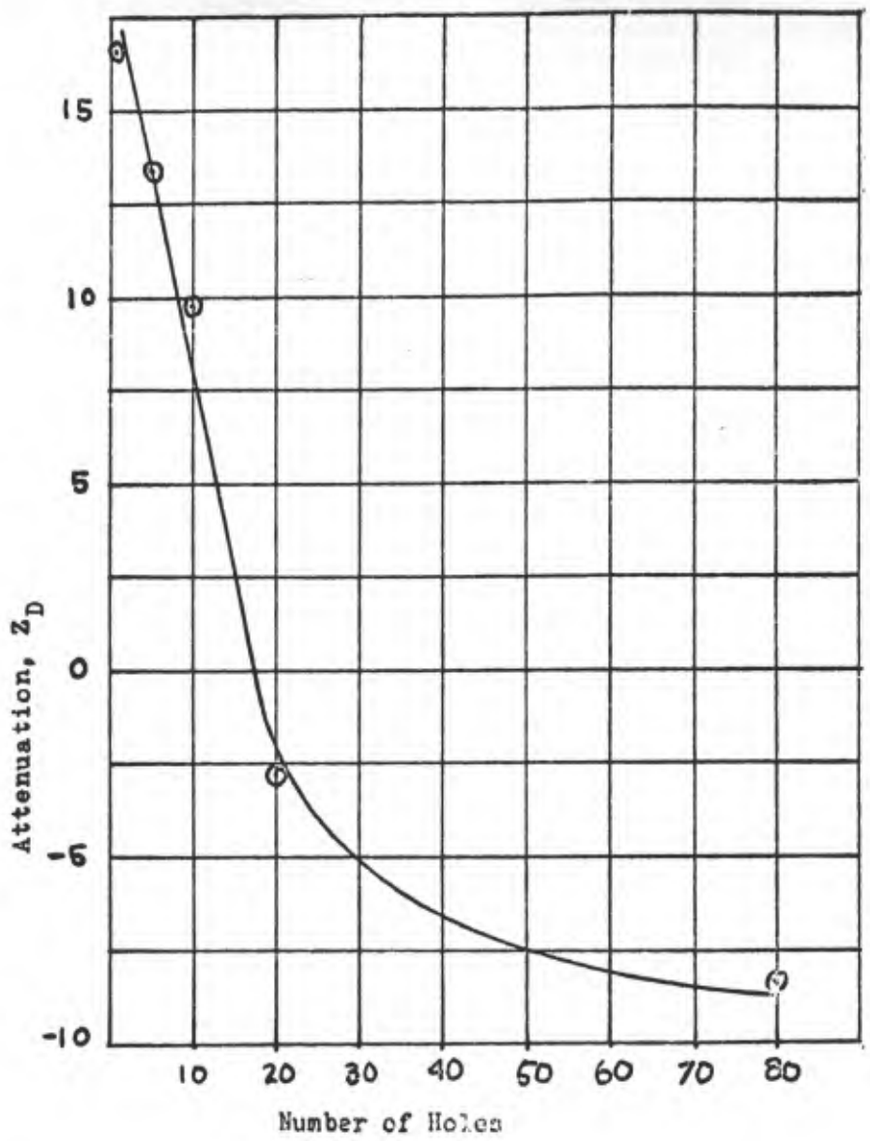

Figure 35. Attenuation vs. Number of Holes, 0.982in.^{2} Open Area Per Plate

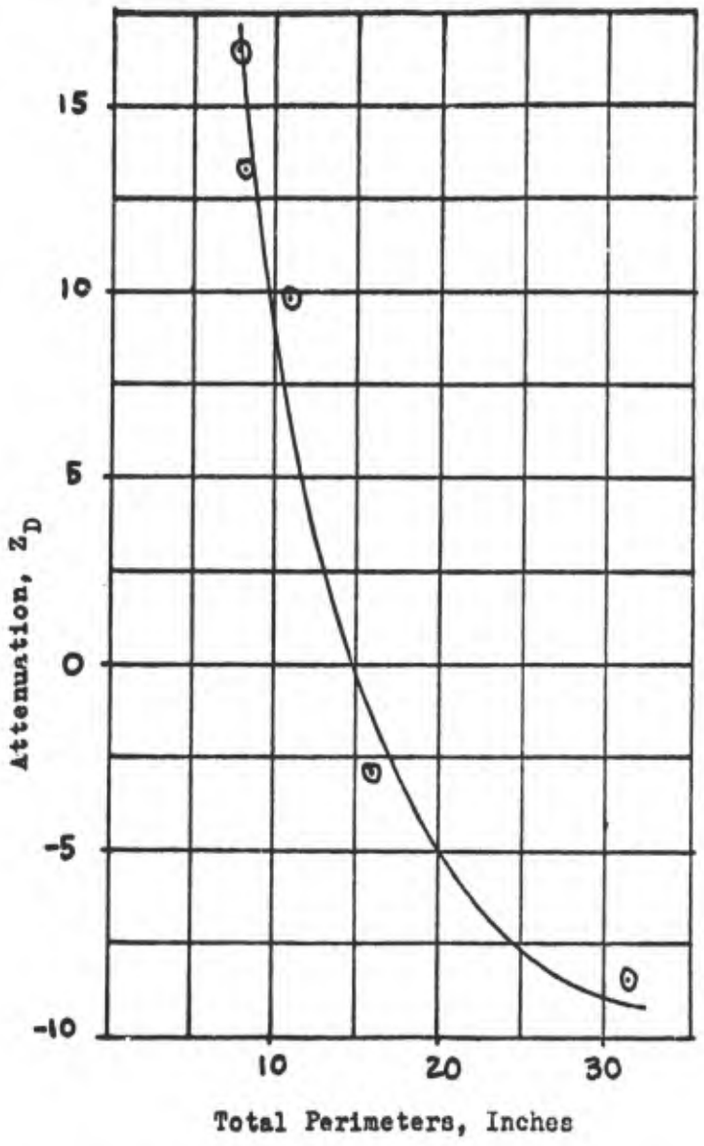

Figure 36. Attenuation vs. Total Perimeters of Holes, 0.982 $in.^2$ Open Area Per Hole

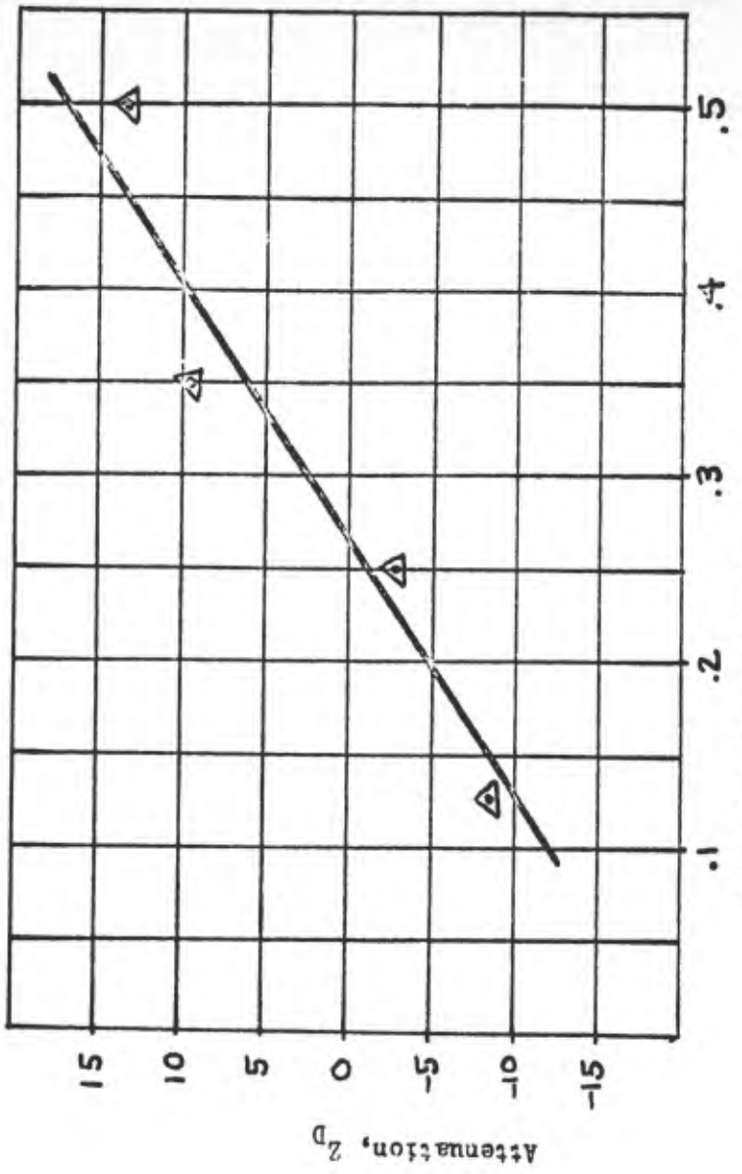

Figure 37. Attenuation vs. Hole Diameter, 0.982 $in.^2$ Open Area Per Plate

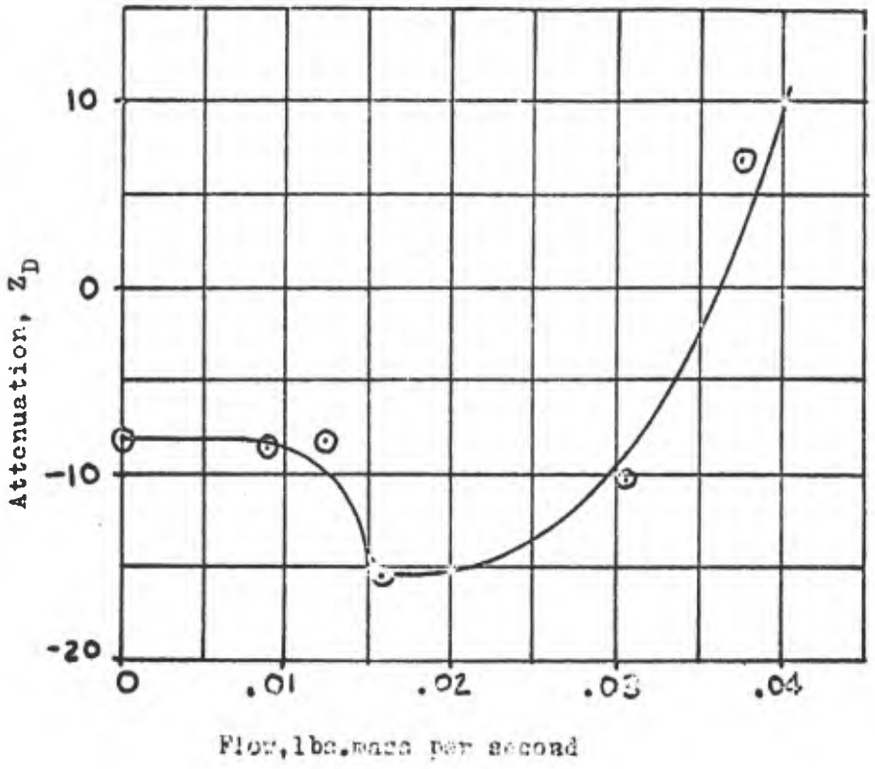

Figure 38. Attenuation vs. Flow in Through 00-0.125 in. Holes Per Plate

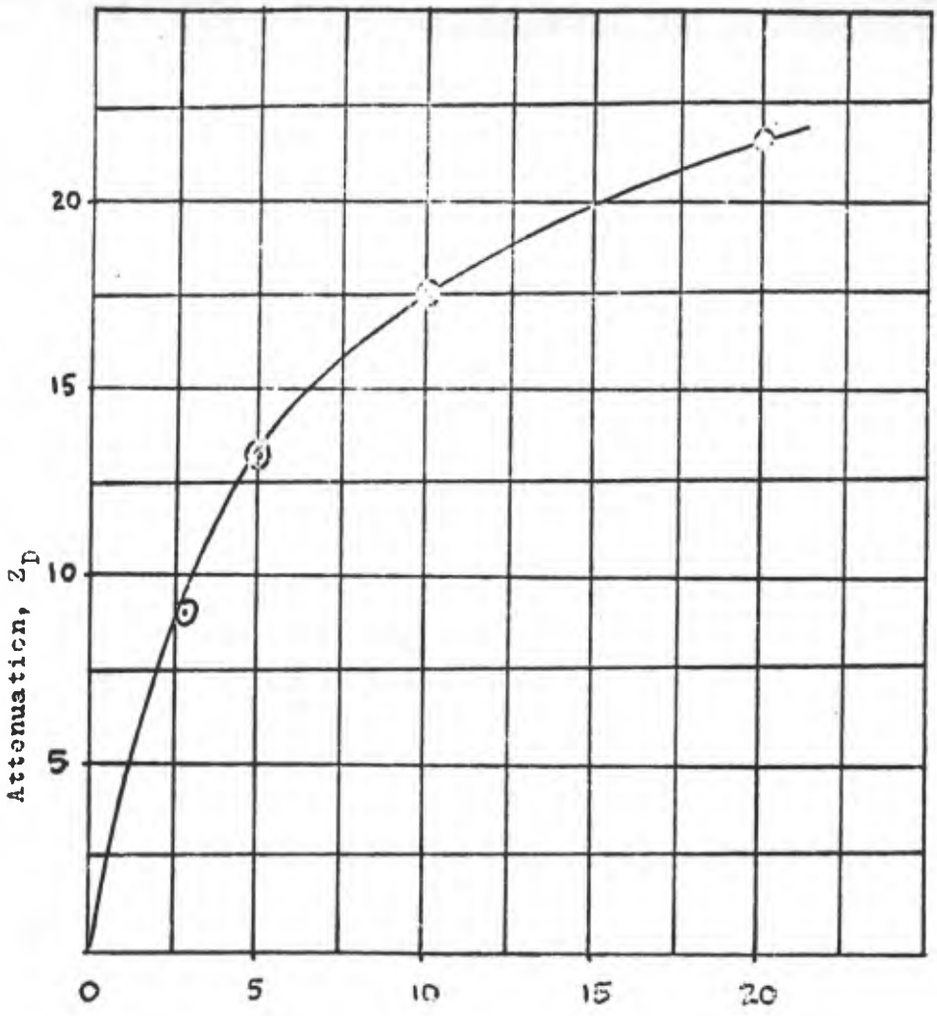

Figure 39.
Attenuation vs. Number of 0.5 in.-Diameter Holes Per Plate

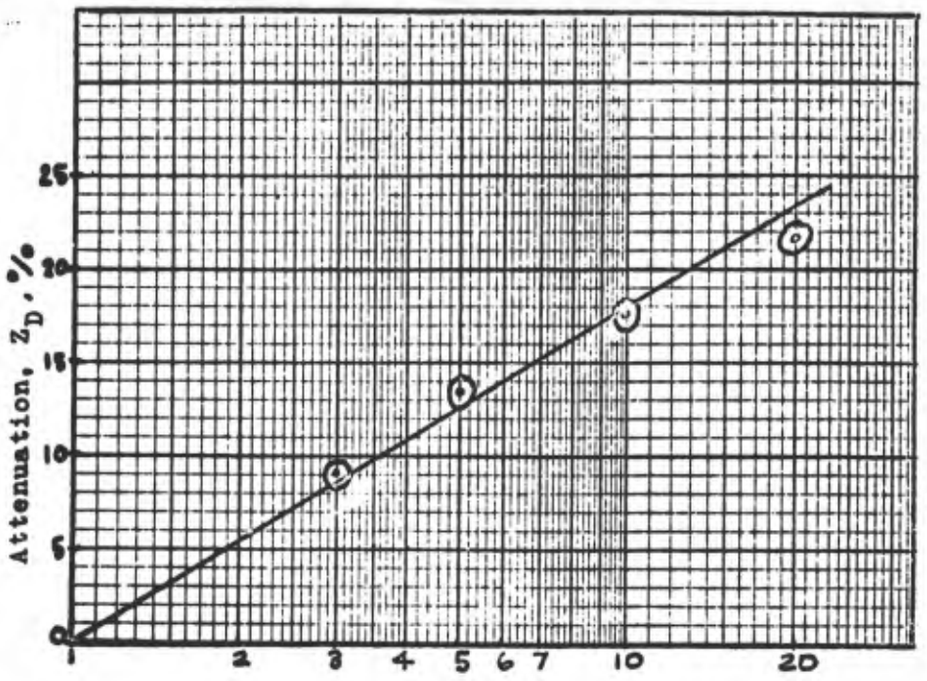

Figure 40. Attenuation vs. Ln. of the Number of 0.5 in. Diameter Holes Per Plate

Appendix A

Sample Calculations for Transducer Calibration

Run No. 1

Initial Readings:

$T_1 = 530^{\circ}R$

$P_1 = 14.57$ psia

Oscilloscope Settings:

Horizontal = .0005 sec/cm.

Vertical = .20 Volts/cm.

Measurements from oscilloscope photograph:

Horizontal sweep distance from start of sweep (station A) to second vertical deflection (station C):

4.60 cm.X .0005 sec/cm = .0023 sec

Vertical deflection from station C:

2.36 cm. X .20 Volts/cm. = .472 Volts

Distance between station A and station C = 3.33 ft.

$W_s = \frac{3.33 \text{ ft.}}{.0023 \text{ sec}} = 1450$ ft./sec

Speed of sound: For air: $C_1 = 49.1 (T_1)^{1/2}$

$C_1 = 49.1 (530)^{1/2} = 1130$ ft/sec

Mach number, $M_s = \frac{W_s}{C_1} = \frac{1450}{1130} = 1.282$

Determining Pressure Step:

From equation (2),

$$P_{21} = \frac{7\,M_s^2 - 1}{6} = \frac{7(1.282)^2 - 1}{6}$$

$$P_{21} = 1.749$$

$$P_2 = 1.749 \times p_1 = 1.749 \times 14.57 \text{ psia}$$

$$P_2 = 25.50 \text{ psia}$$

$$p_2 - p_1 = (25.50 - 14.57) \text{ psi}$$

$$p_2 - p_1 = 10.93 \text{ psi}$$

Corresponding Voltage from transducer #15 = 0.472 Volts.

Appendix B

Sample Calculations For Z_D

Run No. 67

Initial Reading:

$p_1 = 14.45$ psia

From oscilloscope photograph and Figures 22 and 23:

$(p_2-p_1)_C = 10.72$ psi

$(p_2-p_1)_C = 9.80$ psi

Then: $p_{2C} = (p_2-p_1)_C + p_1 = 10.72 + 14.45 = 25.17$ psi

and: $p_{2D} = (p_2-p_1)_D + p_1 = 9.80 + 14.45 = 24.25$ psi

Pressure Ratios:

$$P_{21C} = \frac{P_{2C}}{p_1} = \frac{25.17}{14.45} = 1.740$$

$$P_{21D} = \frac{P_{2D}}{p_1} = \frac{24.25}{14.45} = 1.678$$

Attenuation:

From equation (4),

$$Z_D = \frac{\Delta P_{21}}{P_{21C} - 1} \times 100\% = \frac{P_{21C} - P_{21D}}{P_{21C} - 1} \times 100\%$$

$$Z_D = \frac{1.740 - 1.678}{1.740 - 1} \times 100\%$$

$$Z_D = + 8.4\ \%$$

Vita

Robert MacNair Cameron [redacted] After graduation from Evanston Township High School, Evanston, Illinois in 1944, he entered the United States Army Air Force aviation cadet program. He received his honorable discharge in 1945 at the conclusion of World War II and entered Purdue University in February 1946, where he received his Reserve Commission through the USAF Reserve Officer's Training Corps in June 1948. Upon graduation from Purdue University with a degree of Bachelor of Science in Mechanical Engineering in February 1950, he entered the United States Air Force, where he attended Navigation, Radar, and Bombardment Flying Schools. Prior to entering the Institute of Technology, he served for seven years as a Navigator-Bombardier on the same lead-select B-36 combat crew in the Stategic Air Command.

[redacted]

This thesis was typed by Bette Switalski

UNCLASSIFIED